Title

HIGH-TEMPERATURE PROPERTIES OF SILICATE LIQUIDS: APPLICATIONS TO THE EQUILIBRATION AND ASCENT OF BASIC MAGMA

Author

Carmichael, I.S.E.

Publication Date

1976-08-01

Submitted to Philosophical Transactions of
the Royal Society of London, Series A

LBL-5238
Preprint C. 1

HIGH-TEMPERATURE PROPERTIES OF SILICATE LIQUIDS: APPLICATIONS TO THE EQUILIBRATION AND ASCENT OF BASIC MAGMA

I. S. E. Carmichael, J. Nicholls, F. J. Spera,
B. J. Wood, and S. A. Nelson

August 1976

Prepared for the U. S. Energy Research and
Development Administration under Contract W-7405-ENG-48

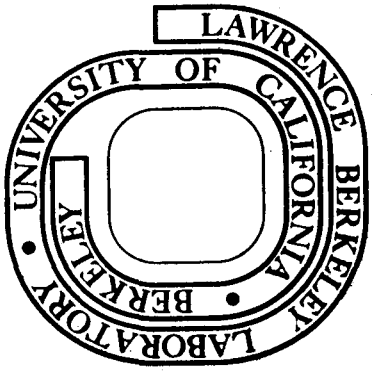

DISCLAIMER

HIGH-TEMPERATURE PROPERTIES OF SILICATE LIQUIDS: APPLICATIONS TO THE EQUILIBRATION AND ASCENT OF BASIC MAGMA

by

I. S. E. Carmichael, J. Nicholls*, F. J. Spera,

B. J. Wood†, and S. A. Nelson

Department of Geology and Geophysics
University of California, Berkeley, California 94720
Lawrence Berkeley Laboratory

High-temperature heat content measurements have been made on a series of silicate liquids, which in conjunction with published data, are used to derive partial molar heat capacities of SiO_2, TiO_2, Al_2O_3, Fe_2O_3, FeO, MgO, CaO, Na_2O and K_2O in the temperature range 1200-1650 K. Only Fe_2O_3 appears to be compositionally dependent, and the best evidence suggests that there is no excess heat capacity ($\bar{C}p_i = C\mathring{p}$). In combination with calorimetric data and the effect of pressure on the fusion temperature of solid compounds, a consistent set of enthalpy, entropy and volume data have been derived for the liquid compounds $CaMgSi_2O_6$, $NaAlSi_3O_8$, $KAlSi_3O_8$, Fe_2SiO_4 and TiO_2.

By using activities (relative to a liquid standard state) calculated at 1 bar for a range of lavas, the equilibration pressures and temperatures of lavas with a lherzolitic source material are calculated, and for basanites indicate 22-25 kbar and 1310-1360°C. The regular solution formulation used in these calculations gives estimated errors of 40°C and 5.7 kbars when compared to experimental equilibria. It is suggested that one of the thermal responses of ascending alkali basalt magma to engulfing cooler lherzolitic nodules could be the precipitation of megacrysts, and the calculated equilibration pressures and temperatures of the megacryst assemblage (16-20 kbar, 1220-1240°C) are in accord with this.

The importance of viewing volcanic eruptions as the last stage in a sequence of chemical and thermomechanical instabilities is pointed out. Equations expressing the conservation of energy, mass and momentum on a macroscopic scale are given. The high Rayleigh numbers appropriate for even the relatively small magma volumes of erupted alkali basalts indicate turbulent flow-regimes with characteristic thermal convection velocities of the same order as nodule settling velocities. There is a significant partial melting effect in the mantle surrounding an ascending diapir if buoyancy is a significant force acting to drive the magma upwards. The effect of latent heat and convective heat losses on the thermal budget of a rising diapir has been calculated and shows the assumption of adiabaticity is often unwarranted -- even for rapidly ascending magma. Finally, mass transfer rates due to convective diffusion have been calculated for all the major components in a basic silicate liquid. Integral mass exchange depends inversely on the ascent rate and is quite small for the rapidly ascending alkalic basalts.

* Department of Geology, University of Calgary, Alberta, Canada

† Department of Geology, University of Manchester

This work was done with support from the U.S. Energy Research and Development Administration.

INTRODUCTION

The liquid state is the essence of igneous petrogenesis, which broadly stated may be conceived of as the generation, ascent and cooling of a silicate liquid. Despite this central role, little is known of the thermodynamic properties of silicate liquids covering the range of composition of those found in nature. This paper, therefore, falls into three parts, the first dealing with measurements of the high temperature heat contents of silicate liquids, from which partial molar heat capacities of the most abundant oxide components found in natural silicate liquids can be obtained. These heat capacity values can in turn be used to derive an internally consistent set of volume, enthalpy and entropy data for liquid silicate compounds based on published information on the effect of pressure on the fusion temperature of these compounds.

In the second part of the paper, these thermodynamic data are applied to naturally occurring silicate liquids or magmas, in order to calculate the equilibration conditions with a stipulated source material in the earth's mantle. The ascent of basaltic magma, particularly through the upper mantle and lower crust is then considered in the third part mainly as an example of a segment of magma history which all to often is ignored in many of today's popular theories of magma genesis. One example will suffice: Mysen and Boettcher (1975) have suggested that almost the whole range of andesitic and basic magmas can be generated by partial fusion of peridotite containing both water and carbon dioxide. But in order to obtain these liquids on the surface of the earth as lavas, an implicit assumption is that the ascent path must allow perhaps 15 weight percent H_2O to be continuously exsolved, a diffusion controlled process, with approximately the same initial and final (eruption) temperature, without changing the composition of the silicate liquid. Such conditions, together with the marked increase in density and viscosity that exsolution would engender can be used to model the time-dependent ascent path, which as more data become available, will allow more constraints to be placed on theories of petrogenesis.

A. Calorimetric Measurements

Many silicate liquids when cooled rapidly below their equilibrium melting point fail to crystallize and become supercooled liquids. Continued cooling of the supercooled liquid causes a discontinuity in the heat capacity (Cp) and the thermal expansion, and the temperature of this discontinuity is called the glass transformation temperature, Tg. In the glass industry, Tg is often defined operationally as the temperature at which the viscosity of the supercooled liquid exceeds 10^{13} poise. As the first-order thermodynamic properties, entropy, enthalpy and volume are continuous at Tg, the supercooled liquid-glass transition is usually accounted a second order transformation, although metastable with respect to the crystalline state. However, the temperature Tg is dependent on cooling rate, and very slow cooling will depress this temperature. For inorganic materials, Tg is often close to the temperature at which Cp (on a gram atom basis) attains the value of 3R; thus Tg may be seen as the temperature at which appreciable translational mobility sets in. For organic polymers (Wrasidlo, 1974), this temperature may frequently be less than 373K, but few silicate compositions have such low temperatures (e.g., Table 2, Bacon, 1976).

High-temperature heat content measurements in the stable liquid region are available for only a few compositions so that a number of glasses were made of various compositions by repeated fusion of crystalline components at high temperatures. Each composition eventually became a homogeneous glass and was then analyzed, with the results set down in Table I. Many of these compositions have been used by Bacon (1976) in his study of heat content and the partial molar heat capacity of oxide components in the glass region (i.e., below Tg).

For measurement of heat content in the glass-supercooled liquid region, 7 to 9 grams of glass (50-100 mesh) were loaded into Pt-10Rh capsules (2 cm. diameter and 2.5 cm. long), evacuated, and sealed by arc-welding under 1 atmosphere of argon. The sample container was suspended by 0.25 mm Pt-10Rh wire in a vertical Pt-wound furnace. Temperature was measured with Pt/Pt-10Rh thermocouple placed just above the top of the container. The thermocouple was calibrated frequently at the melting temperature of Au (1063°C), and the small corrections were assumed to be linear over the experimental temperature range (400-1650K). Reported temperatures are believed to be accurate to ±1°.

After the sample had reached thermal equilibrium in the furnace, two sets of gates shielding the bottom of the furnace and the top of the calorimeter were opened momentarily, and the sample dropped on its suspension wire in less than 1 second into the calorimeter well. The calorimeter consists of a copper tube with horizontal fins enclosed in a double wall glass vessel immersed in a waterbath maintained at a constant temperature (±.001°), slightly above the melting temperature of diphenyl ether (300.03K). The space between the copper tube and the glass wall is filled with diphenyl ether, part of which is frozen into a crystalline mantle completely surrounding the horizontal fins. A pool of mercury in the bottom of the glass vessel connects with a calibrated horizontal capilliary.

A hot sample introduced into the calorimeter melts some of the diphenyl ether, and forces mercury along the capilliary, and the amount displaced is directly proportional to the heat content (H_T-H_{300}) of the sample at the instant it entered the calorimeter. The calorimeter constant is assumed to be 18.91 cals per gram of mercury displaced (Jessup, 1955).

The heat content of the Pt-10Rh container and suspension wire, and the heat lost during the drop, were accounted for by measuring the heat content of an empty container of similar size and shape, so that small differences in mass between containers could be corrected for by assuming that the heat content of an empty capsule is directly

TABLE 1

Analysis of Prepared Compositions

	#7	#8	#9	#12	#66	#114	#121
SiO_2	39.37	54.11	63.1	63.96	73.5	57.7	70.5
TiO_2	-	20.00	-	-	0.30	0.93	0.32
Al_2O_3	11.80	-	-	-	13.6	15.5	7.77
Fe_2O_3	1.61	-	-	-	1.92	9.99	9.14
FeO	41.39	-	-	-	-	-	-
MnO	0.03	-	-	-	0.02	0.18	0.24
MgO	-	-	14.0	10.58	0.32	3.50	0.03
CaO	5.99	-	-	-	1.24	6.91	0.35
Na_2O	-	25.45	22.9	-	4.04	3.99	6.88
K_2O	-	-	-	25.39	4.27	1.29	4.15
P_2O_5	-	-	-	-	0.03	0.26	0.01
MoO_3	-	-	-	-	0.02	0.24	0.35
Gram formula weight	68.418	63.759	56.592	62.592	65.578	67.867	67.450
Gram atom/ formula weight	2.7052	3.000	2.8034	2.8356	3.1726	3.1524	3.1753
Gram atom/gram	.03954	.04705	.04954	.04530	.04838	.04645	.04708

proportional to its mass, as all the Pt-10Rh components are similar.

For runs made from the stable liquid region (1200-1650K), the mass of silicate material in the 2 x 2.5 cm. containers was too large to recover glass and the sample partially devitrified while cooling in the calorimeter. Smaller containers of Pt-10Rh, 1 cm. diameter and 2 cm. long, were made for these high-temperature runs, and cooling in the calorimeter of the 1-1.5 grams of silicate material they contained was sufficiently rapid to recover the same glassy state, in terms of its heat content, as the glass which had been synthesized and used for experiments below and above Tg. Again the heat content of the empty small container was measured over a wide range of temperatures, but per unit mass was lower than for the large capsules.

Reproducibility of individual runs was generally within ±0.3% of the measured heat content, and a few runs were made on the National Bureau of Standards sapphire sample #720. Those runs made in the large containers matched those of Bacon (1976) which would suggest an accuracy of about ±0.5% in heat content and ±1% in heat capacity. Measurements of the heat content of sapphire in the small capsules were systematically low over a wide temperature range, and a small temperature dependent correction was applied to all measurements made in the small capsules; this correction invariably produced excellent agreement with runs on the same composition made in the large containers over the same temperature range, i.e., just above Tg.

Of the errors that could arise, the calculated contribution of the Ar gas to the measured heat content of the sample was so small that it was ignored. At high temperatures, Fe is soluble in Pt-10Rh and doubtless some of the FeO in the silicate liquid will dissolve in the containers, liberating oxygen. The FeO-rich sample (composition #7) was held for only a minimum time in the furnace before dropping; duplicate runs made at the end of the sequence of experiments, when presumably the solution of Fe in the container was more advanced, showed no detectable change in heat-content.

The normal experimental procedure was to initially use the large capsules containing 7-9 grams of the silicate composition, and measure the heat content of the sample at successively increasing temperatures (~50K) until Tg was reached. This is most easily shown by plotting $(H_T-H_{300})/(T-300)$ against T, and an example of this type of plot is shown in Figure 1 for composition #12. There is a clear change in slope of the mean specific heat curve at Tg. Each run in the supercooled liquid region, i.e., above Tg, was followed by a run in the temperature range of the glass region to ensure that partial devitrification had not occurred, either in the furnace or in the calorimeter. The large capsules were abandoned once partial devitrification set in, and a set of measurements from the stable liquid region was made in small capsules, with a few runs made from the supercooled liquid region to ensure that the two sets of results were concordant.

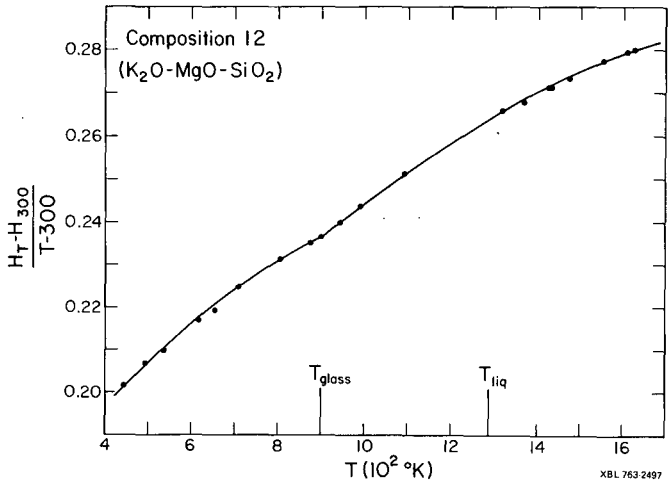

Fig. 1. Values of mean specific heat (H_T-H_{300}/T-300) in cal./gm. for composition #12 plotted against TK. Temperatures of the glass transformation, Tg, and the liquidus temperature are also shown.

For compositions of relatively low viscosity, and low value of Tg, there is a large temperature interval which is experimentally inaccessible between the last supercooled liquid run and the lowest temperature run from the stable liquid region. In this inaccessible region, devitrification or partial crystallization is prevalent, and cannot be prevented with the present experimental conditions; for some compositions this interval is over 600K (Table 2).

The results for the seven compositions are given in Table 2 but for compositions 7, 66, 121 and 114 only the stable liquid data are given, as Bacon (1976) has determined the heat contents of these four compositions in the glass and supercooled liquid region. However, we have ensured that in compositions 66, 121 and 114 all the FeO was oxidized to Fe_2O_3 by holding each composition open to the atmosphere at 800K for 24 hours followed by re-weighing the sample; the gain in weight was approximately what was expected. Thereafter the containers were crimped shut and weighed after each run to ensure that the composition remained constant.

Equations of heat content ($H_T-H_{298.15}$)

The heat contents in the stable liquid region for the seven compositions given in Table 2 can all be fitted by two term equations to within ±0.22% or less (Table 3) which is smaller than the experimental reproducibility. The only possible exception is composition 66, but although the fit is poorer than for all the other compositions, it is still within the experimental error. A small correction to the constant changes the reference temperature to 298.15K.

Differentiation of the high-temperature heat content equations given in Table 3 gives the heat capacity at constant pressure Cp, on a per gram basis. Although within the experimental temperature range of 1200-1650K, Cp is essentially independent of temperature, it is likely that over a larger temperature range, there will be a measurable temperature dependence of Cp, and it may be expected to decrease slightly.

Also shown in Table 3 are fit equations for the heat content for the supercooled liquid region for the three compositions 8, 9 and 12. It is clear that Cp in the supercooled liquid region is quite different to that in the stable liquid region, so that all subsequent calculations have used only published data where it can be established that the heat content data is for the stable liquid region.

We wish to be able to express the heat capacity of any silicate liquid in terms of its constituent oxides to that

$$Cp_{liquid} = \sum_i X_i a_i$$

where a_i is the coefficient of the i^{th} component, and X_i the mole of fraction of i. As a first step, the compositions given in Table 1 have to be recalculated onto a normalized gram formula weight basis with the sum of the oxide components equal to unity. As an example, we may use the composition Fe_2SiO_4 for which we have

Weight	Percent	Molecular Proportions	Molecular Fraction
SiO_2	29.49	.4908	.3334
FeO	70.51	.9814	.6666

Gram Formula Weight	Gram Atoms/ Formula Weight
.3334 x 60.085 = 20.03	.3334 x 3 = 1.0000
.6666 x 71.846 = 47.89	.6666 x 2 = 1.3333
Sum 62.92	2.3333

and Gram atom/gram of Fe_2SiO_4 = 2.3333/67.92 = .03436.

and the corresponding data for all the compositions are given in Table 1. Note that the normalized gram formula weight as expressed here for Fe_2SiO_4 is not that conventionally given for Fe_2SiO_4 where the sum of the oxide components is equal to three rather than unity. All the measured heat capacities on a per gram basis in Table 3 require to be multiplied by the gram formula weight of each composition to put them on a comparable basis. The molecular weights we have used are given in Table 4. Before the final calculation was performed, the appropriate amount for the contribution of MoO_3 (from the fusion crucible), P_2O_5 and MnO was subtracted from the gram formula weight heat capacity. The values used were MoO_3 (liquid) = 32.00; P_2O_5 (liquid) = 58.5 (Kelley, 1960) and for Cp_{MnO} (liquid) we used a value of 19.08 cals $mole^{-1}$ deg^{-1} which was derived from Mah's (1960) data on liquid Mn_2SiO_4 and our data for SiO_2 (Table 5).

TABLE 2

$H_T - H_{300}$ for Compositions listed in Table 1

Data in Calories Per Gram

Composition 8

Run No.	T°K	$H_T - H_{300}$
	Glass Region (Tg = 468 K)	
7	420.8	26.51
8	421.2	26.56
9	479.0	39.61
10	480.1	39.95
13	461.9	35.65
	Supercooled liquid region	
239	644.8	81.80
243	618.6	74.68
242	588.3	66.98
240	563.8	60.57
241	532.2	52.49
11	596.5	69.02
14	529.2	51.98
20	492.4	43.03
9	479.0	39.61
10	480.1	39.95
	Stable liquid region (>1150K)	
230	1236.4	287.80
229	1456.6	364.94
228	1628.0	423.64
227	1265.1	297.88
226	1578.6	406.85
225	1312.4	315.36
224	1386.0	339.69
223	1522.1	387.38
221	1434.9	357.47

Composition 9

Run No.	T°K	$H_T - H_{300}$
	Glass Region (Tg = 496K)	
32	480.0	40.93
33	466.6	37.77
37	455.9	35.29
39	451.1	34.17
	Supercooled liquid region	
248	645.3	86.46
244	618.8	78.49
247	584.4	68.51
246	557.3	60.87
245	528.6	53.23
34	512.4	49.10
35	575.3	66.17
	Stable liquid region (>1200K)	
219	1479.0	377.85
218	1423.1	356.09
216	1262.9	297.06
214	1542.9	401.72
213	1351.5	328.96
212	1506.4	388.39
211	1320.8	318.47
209	1635.5	434.63
208	1507.6	389.06
207	1388.1	342.38

Composition 7

Run No.	T°K	$H_T - H_{300}$
	Stable liquid region (>1375K)	
258	1482.3	327.23
266	1430.1	313.18
265	1457.6	320.93
264	1500.5	333.12
263	1499.4	331.96
262	1407.1	306.51
261	1595.3	361.65
260	1541.8	346.99
259	1655.7	380.99

Composition 66

Run No.	T°K	$H_T - H_{300}$
	Stable liquid region (>1300K)	
274	1306.7	272.88
279	1345.6	285.40
278	1408.8	308.25
275	1482.7	332.30
277	1537.4	350.55
280	1590.7	366.72
276	1640.7	381.51

Composition 12

Run No.	T°K	$H_T - H_{300}$
	Glass Region (Tg = 900K)	
42	440.3	28.32
43	493.2	39.91
46	646.0	75.89
48	533.9	49.08
49	616.8	68.72
50	708.6	91.83
51	804.8	116.79
52	900.0	141.81
57	875.6	135.28
	Supercooled liquid region	
53	989.6	168.18
55	944.5	154.69
56	1090.3	198.67
	Stable liquid region (>1286K)	
206	1556.1	348.40
205	1430.6	306.84
204	1621.8	369.74
202	1609.8	365.81
201	1368.6	286.20
200	1319.4	271.04
198	1485.1	324.04
196	1422.1	304.44

Composition 114

Run No.	T°K	$H_T - H_{300}$
	Stable liquid region (>1400K)	
273	1663.0	405.41
272	1602.6	384.41
271	1431.3	324.42
270	1507.5	352.03
269	1545.8	365.25

Composition 121

	Stable liquid region (>1300K)	
291	1436.1	330.60
290	1313.0	389.00
289	1544.0	368.09
288	1596.2	386.24
285	1637.6	400.38
283	1349.6	299.76
282	1542.2	366.82

All runs with numbers above 100 were made in small (1 cm dia x 2 cm length) containers; remainder in large containers.

In addition to the data of Table 3, the heat capacities for liquid Fe_2SiO_4 (Orr, 1952), liquid $CaTiSiO_5$ (King et al. 1954), liquid Na_2SiO_3 (Naylor, 1945), liquid $K_2O \cdot 2 \cdot 5SiO_2$ and $Na_2O \cdot CaO \cdot 6SiO_2$ (Schweite and Ziegler, 1955) were also included and the whole array fitted by least-squares in an over determined matrix of 13 data sets to give values of $\bar{C}p_i$, the partial molar heat capacities for each of the nine liquid oxide components.

These are listed in Table 5 together with the calculated value of one standard deviation (σ) and the concentration range of each oxide component in the data set. Using these partial molar heat capacity values, the calculated values may be compared to the observed values for the data set together with the percentage difference and are given in Table 6.

The magnitude of the standard deviation for each estimated value of $\bar{C}p_i$ is clearly related to the range of concentration and each oxide component (Table 5). The greatest uncertainties are for Al_2O_3 and Fe_2O_3, and both estimates for $\bar{C}p_i$ require extensive extrapolation in terms of composition (e.g., for Fe_2O_3 from 0.04 to 1.00).

It seems likely that $\bar{C}p_{Fe_2O_3}$ is compositionally dependent, and as the concentration of Fe_2O_3 increases, the value would fall to an anticipated value close to 2.5 $\bar{C}p_{FeO}$. Although the uncertainty in $\bar{C}p_{Fe_2O_3}$ is very large, this is only of significance if this value is used to calculate the heat capacity of a liquid in which Fe_2O_3 is a major component; for natural silicate liquids with very small amounts of Fe_2O_3, the value in Table 5 is appropriate for it was derived from such compositions.

With the exception of Fe_2O_3 and possibly of Al_2O_3, the results in Table 5 and Table 6 show that within the composition range represented by the experimental compositions.

$$\bar{C}p_i = Cp_i$$

if i is taken as Fe_2SiO_4 or $CaTiSiO_5$; in other words, there is no excess heat capacity for these two components. If other components are chosen this conclusion is less easily substantiated, and possibly not experimentally capable of proof. For example the measurement of the heat capacity of pure liquid K_2O ($Cp°_{K_2O}$) is fraught with enormous difficulties so that it may be impossible ever to establish that

$$Cp_{K_2O} = Cp°_{K_2O}$$

Similarly the heat capacity of pure liquid MgO has been calculated in the temperature range 3098-3873K (Leu et al., 1975), and it would require only a small temperature dependence of $Cp°_{MgO}$ (~23.81) to match $\bar{C}p_{MgO}$ in the temperature range 1200-1650K. Lastly two sets of measurements of $Cp°_{Al_2O_3}$ are available; one value is 34.623 (Janaf, 1971) and a later value by Shpil'rain

TABLE 3

Heat Content ($H_T - H_{298.15}$) Equations for the Compositions Investigated. Data in cals per gram.

Composition	$H_T - H_{298.15}$	Temp. Range		Mean % Deviation
7	0.3000T - 116.235	1400 - 1655K	stable liquid	0.22
8	0.3467T - 140.075	1236 - 1628K	stable liquid	0.11
8	0.2527T - 81.188	470 - 645K	supercooled liquid	0.39
9	0.3734T - 174.539	1260 - 1636K	stable liquid	0.18
9	0.2813T - 95.513	512 - 645K	supercooled liquid	0.49
12	0.3278T - 161.735	1319 - 1621K	stable liquid	0.11
12	0.3018T - 130.122	990 - 1090K	supercooled liquid	0.03
66	0.3278T - 154.308	1307 - 1641K	stable liquid	0.30
121	0.3455T - 165.296	1313 - 1640K	stable liquid	0.13
114	0.3483T - 173.217	1431 - 1663K	stable liquid	0.11

The mean deviation is the average percentage deviation of the smoothed heat content values from those measured.

et al. (1972) shows that the heat capacity is temperature dependent in the range 2323-3100K with a mean value near 46.03. Clearly the data on the pure liquid oxides, which are experimentally extremely difficult to obtain, can really not be used to show that $\bar{C}p_i \neq Cp_i^\circ$, and in what follows we shall assume that there is no excess heat capacity no matter which oxide component is chosen, despite the fact we have only been able to establish this for Fe_2SiO_4 and $CaTiSiO_5$.

The unwary reader may consider that it should be possible to use the individual heat content measurements (Table 2) and from these derive partial molar heat contents for each oxide, and then by differentiation obtain the partial molar heat capacities. Such a procedure requires that the same reference state at 298.15K, glass or crystals, be common to the data set; the two reference states cannot be mixed as the following

TABLE 4

Molecular Weights Used in the Calculation of Partial Molar Heat Capacities

SiO_2	60.0848
TiO_2	79.8988
Al_2O_3	101.9612
Fe_2O_3	159.6922
FeO	71.8464
MnO	70.9374
MgO	40.3044
CaO	56.0794
Na_2O	61.9790
K_2O	94.2034
P_2O_5	141.9446
MoO_3	143.9382

TABLE 5

Partial Molar Heat Capacities (cals/mole.deg) in Silicate Liquids in the Temperature Range 1200-1650K

	$\bar{C}p_i$	σ	X_i
SiO_2	20.79	0.16	0.81 to 0.33
TiO_2	26.74	0.58	0.33 to 0.0
Al_2O_3	24.64	1.43	0.10 to 0.0
Fe_2O_3	78.64	3.53	0.04 to 0.0
FeO	18.34	0.18	0.67 to 0.0
MgO	21.62	0.54	0.20 to 0.0
CaO	19.32	0.64	0.33 to 0.0
Na_2O	22.00	0.33	0.50 to 0.0
K_2O	17.73	0.58	0.29 to 0.0

Note that the following values of partial molar liquid heat capacities have been assumed in the calculations: MnO = 19.08; P_2O_5 = 58.5; MoO_3 = 32.00.

TABLE 6

Comparison of Observed and Calculated Heat Capacities

(calories/normalized gram formula weight deg.)

Composition	Observed C_p	Calculated C_p	% Difference
Fe_2SiO_4	19.10	19.16	0.3
$CaTiSiO_5$	22.27	22.29	0.1
Na_2SiO_3	21.41	21.40	0.05
#7	20.52	20.42	0.5
#8	22.11	22.06	0.2
#9	21.13	21.21	0.4
#12	20.52	20.41	0.5
#66	21.48	21.54	0.3
#121	23.21	23.16	0.2
#114	23.50	23.54	0.2
$K_2O \bullet 2.5SiO_2$	19.86	19.92	0.3
$Na_2O \bullet CaO \bullet 6SiO_2$	20.84	20.76	0.4
Wirtschaftsglas	20.88	20.95	0.3

Average deviation = 0.29%

equations illustrate. Cooling in the calorimeter liberates an amount of heat which is quite different depending on whether the sample is cooling to crystals or to glass. Heat liberated in cooling from T to glass reference state at 298.15 is given by

$$= H_T - H_{Tg} + \int_{298}^{Tg} Cp_{glass}\, dT \qquad (1)$$

whereas the heat liberated in cooling from T to a crystalline reference state at 298.15 is given by

$$= H_T - H_{Tm} + \Delta H_{crystal.} + \int_{298}^{Tm} Cp_{solid}\, dT \qquad (2)$$

where Tg, Tm and $\Delta H_{crystal}$ refer to the glass transformation temperature, the equilibrium melting temperature and the heat of crystallisation, respectively.

Until more data is available such a procedure has been rejected as it would require that the crystalline reference state data (e.g. Fe_2SiO_4, $CaTiSiO_5$) be ignored; thus we have of necessity focused on heat capacity and neglected the heat content data.

Thermodynamic Data for Liquid Compounds

One use to which this liquid heat capacity data may be put is to derive an internally consistent set of enthalpy and volume data for liquid compounds if the equilibrium between solid and liquid is known as a function of pressure.

For the reaction

$$\text{solid} \rightleftarrows \text{liquid}$$

we may write at equilibrium along the fusion curve

$$\Delta G = 0 = \Delta H_{Tr} + \int_{Tr}^{T} (Cp_{liq} - Cp_{solid})\, dT - T\left[\Delta S_{Tr} + \int_{Tr}^{T} \frac{(Cp_{liq} - Cp_{solid})}{T}\, dT\right] + \int_{1}^{P} \Delta V dP \qquad (3)$$

where ΔH_{Tr}, ΔS_{Tr}, ΔV are the enthalpy, entropy and volume of fusion of 1 mole of solid at the 1 bar melting temperature. The variation of the volume with P and T is conveniently expressed as

$$V_{solid} = (a_s T + b_s)(1 - \beta P)$$

where β is the isothermal compressibility of the solid. For the liquid

$$V_{liquid} = (a_L T + b_L + c_L P)$$

where c_L is dV_{liquid}/dP.

If the slope of the fusion curve is known at 1 bar then it is possible to estimate either the heat or volume of fusion from the Clapeyron relationship

$$(dT/dP)_{1bar} = \frac{T\Delta V_{fusion}}{\Delta H_{fusion}}$$

We set out in Table 7 the thermodynamic data on liquid compounds which have been derived using equation (3) coupled with the fusion curves.

TABLE 7

Thermodynamic Data for Liquid Compounds

Precision and accuracy of the following data are not established and the number of decimal places is only given to avoid significant round-off errors.

Fe_2SiO_4

Cp liquid = 57.30 (Orr, 1953)

Cp solid = $36.51 + 9.36 \times 10^{-3}T - 6.70 \times 10^{5}T^{-2}$ (Kelley, 1960)

ΔH_{fusion} = 22030 cals (Orr, 1953)

T_{fusion} = 1490K

ΔS_{fusion} = 14.785 cals/mole.deg.

$V_{solid} = (31.43 \times 10^{-6}T + 1.0996)(1-0.91 \times 10^{-6}P)$ (Skinner 1966 and Birch, 1966)

$V_{liquid} = (101.75 \times 10^{-6}T + 1.0822 - 1.94 \times 10^{-6}P)$

where a_L and b_L are taken from Bottinga and Weill (1970) and c_L comes from fitting the fusion curve of Lindsley (1967). The calculated fusion curve in relation to the experimental curve is shown in Figure 2.

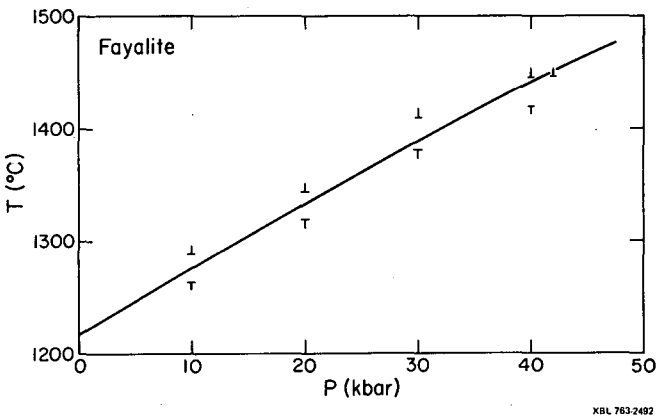

Fig. 2. The experimental brackets for the fusion curve of Fe_2SiO_4 (Lindsley, 1967) together with the calculated curve.

$NaAlSi_3O_8$

Cp_{liquid} = 85.69 (Table 5)

$Cp_{solid} = 61.70 + 13.90 \times 10^{-3}T - 15.01 \times 10^{5}T^{-2}$ (Kelley, 1960)

$Cp_{glass} = 61.31 + 18.00 \times 10^{-3}T - 16.16 \times 10^{5}T^{-2}$ (Kelley, 1960)

T_{fusion} = 1391K

For albite (xals) → albite (glass), ΔH_{298} = 11904 cals (Robie & Waldbaum, 1968)

Given Tg at 1036K (Arndt & Haberle, 1973) then ΔH_{fusion} at 1391K is found by integration of

$$\Delta H_{fusion} = \Delta H_{298} + \int_{298}^{1036} (Cp_{glass} - Cp_{xals})dT + \int_{1036}^{1391} (Cp_{liq} - Cp_{xals})dT = 16258$$

cals.

ΔS_{fusion} = 11.688 cals/mole.deg.

$V_{solid} = (67.66 \times 10^{-6}T + 2.377)(1-1.48 \times 10^{-6}P)$ (Skinner 1966, Birch, 1966)

$V_{liquid} = (171.91 \times 10^{-6}T + 2.3727 - 7.49 \times 10^{-6}P)$ which comes from fitting the fusion curve of Boyd and England (1963).

The calculated fusion curve in relation to the experimental brackets is shown in Figure 3.

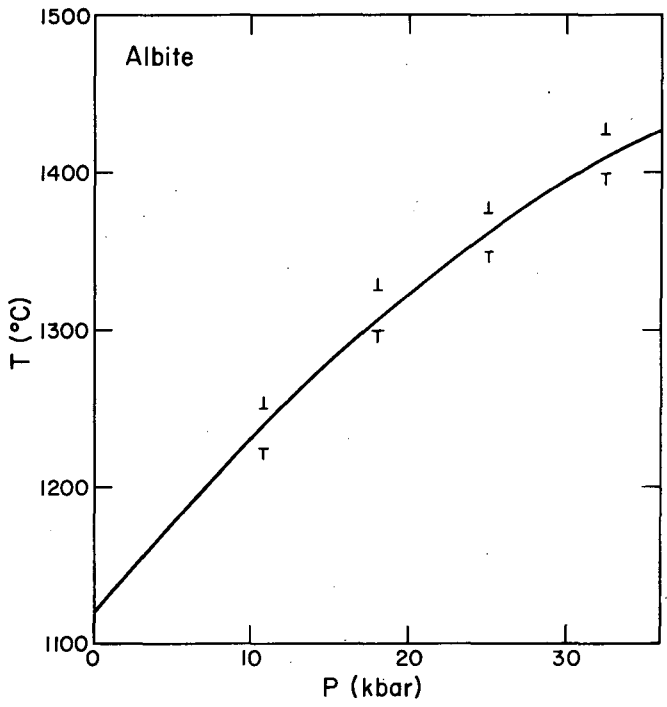

Fig. 3. Experimental brackets on the $NaAlSi_3O_8$ fusion curve (Boyd and England, 1963) and the calculated curve.

$CaMgSi_2O_6$

Cp_{liquid} = 82.52 (Table 5)

$Cp_{solid} = 52.87 + 7.84 \times 10^{-3}T - 15.74 \times 10^{5}T^{-2}$ (Kelley, 1960)

T_{fusion} = 1664K

ΔH_{fusion} = 31043 cals obtained from density of liquid $CaMgSi_2O_6$ (Skinner 1966) and dP/dT of fusion curve (Rosenhaum and Eggler, 1975)

ΔS_{fusion} = 18.656 cals/mole.deg.

V_{solid} = $(46.27 \times 10^{-6}T + 1.5644)(1-1.07 \times 10^{-6}P)$ (Skinner, 1966 and Birch, 1966)

V_{liquid} = $(178.25 \times 10^{-6}T + 1.6083 - 7.26 \times 10^{-6}P)$

which comes from fitting the fusion curve of Boyd and England (1963). The calculated value of ΔH_{fusion} is within the measured value (30700 ± 800 cals) of Ferrier (1970). The calculated fusion curve in relation to the experimental points is shown in Figure 4.

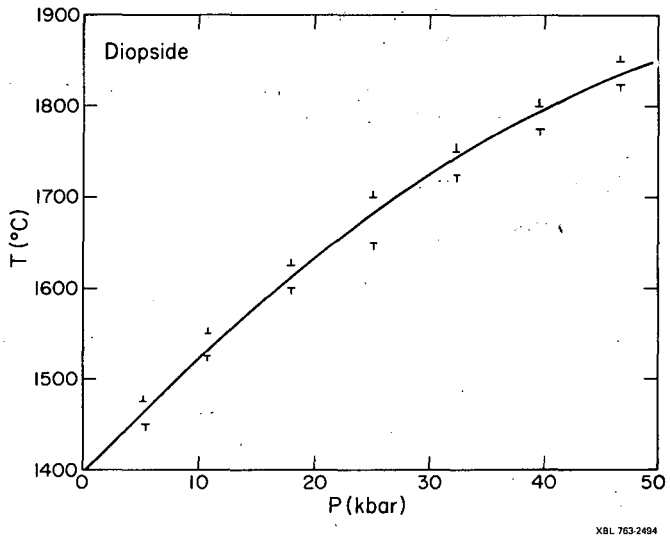

Fig. 4. Experimental brackets on the $CaMgSi_2O_6$ fusion curve (Boyd and England, 1963) and the calculated curve.

$KAlSi_3O_8$

Cp_{liquid} = 83.56 (Table 5)

Cp_{solid} = $63.83 + 12.90 \times 10^{-3}T - 1705 \times 10^{5}T^{-2}$ (Kelley, 1960)

Cp_{glass} = $61.96 + 17.16 \times 10^{-3}T - 14.29 \times 10^{5}T^{-2}$ (Kelley, 1960)

T_{fusion} = 1473K

For sanidine (xals → sanidine (glass), ΔH_{298} = 11102 cals (Robie & Waldbaum, 1968)

Given Tg = 1178K (Arndt and Haberle, 1973), then ΔH_{fusion} at 1473K is found by integration of

$$\Delta H_{fusion} = \Delta H_{298} + \int_{298}^{1178} (Cp_{glass} - Cp_{xals})dT + \int_{1178}^{1473} (Cp_{liq} - Cp_{xals})dT = 13980 \text{ cals}$$

ΔS_{fusion} = 9.491 cals/mole.deg.

V_{solid} = $(70.94 \times 10^{-6}T + 2.5795)(1-1.76 \times 10^{-6}P)$ (Skinner, 1966 and Birch 1966)

V_{liquid} = $(78.03 \times 10^{-6}T + 2.7442 - 9.88 \times 10^{-6}P)$

which comes from fitting the three data points of Lindsley's (1966) fusion curve. The calculated fusion curve, metastable below 19.6 kbars, is shown in relation to the experimental brackets in Figure 5.

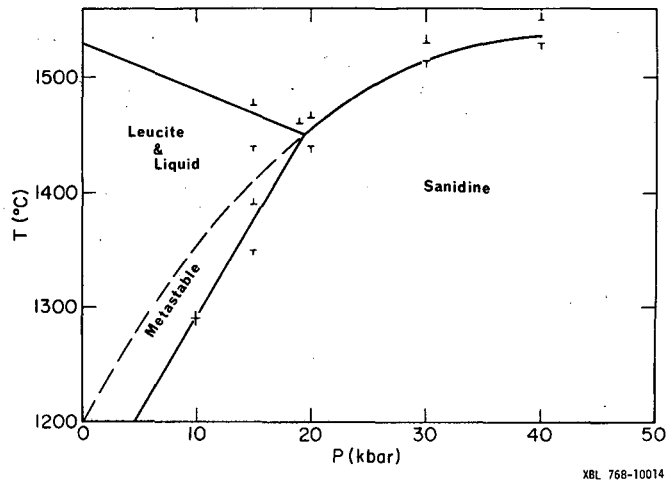

Fig. 5. Experimental brackets on the $KAlSi_3O_8$ fusion curve (Lindsley 1966) and the calculated curve which is metastable below 19 kbars.

TiO_2

Cp_{liquid} = $26.74 - 1.25 \times 10^{-3}T$ (Table 5 with a temperature dependence on Cp within the limits of Table 5).

Cp_{solid} = $17.97 + 0.28 \times 10^{-3}T - 4.35 \times 10^{5}T^{-2}$ (Kelley, 1960).

T_{fusion} = 2103K but JANAF (1975) give the stoichiometric melting temperature as 2130K; the value here is taken from Robie and Waldbaum (1968).

ΔH_{fusion} = 10,000 cals (estimated)

ΔS_{fusion} = 4.755 cals/mole.deg.

V_{solid} = $(12.26 \times 10^{-6}T + 0.4460)(1 - 0.51 \times 10^{-6}P)$ (Skinner, 1966 and Birch 1966)

V_{liquid} = $(55.97 \times 10^{-6}T + 0.3887 - 1.04 \times 10^{-6} P)$

which is taken from fitting the fusion curve estimated from MacGregor (1969).

Al_2O_3

Cp_{liquid} = 40.32 (Average of JANAF 1974 and Shpil'rain et al. 1972)

T_{fusion} = 2327K

ΔH_{fusion} = 28000 cals (JANAF 1974)

ΔS_{fusion} = 12.033 cals/mole deg.

V_{liquid} = $330.99 \times 10^{-6}T + 0.03986 - 11.78 \times 10^{-6}P$ (Kirshenbaum and Cahill, 1960). The value of $(dV/dP)_T$ is very uncertain in view of the range in the measured values of Cp of Al_2O_3 liquid, for it is derived from Slagle and Nelson's date (1970) on the adiabatic compressibility of Al_2O_3 liquid. Choosing the mean value of Cp (above), β_T becomes zero at 1944K, which is impossible, so we have used the mean value in the experimental temperature range to obtain $(dV/dP)_T$.

These data together with that of JANAF (1974) for solid Al_2O_3 (i.e. $\Delta H°_{f\ 298} = -400500$ cals and $S°_{298} = 12.18$ cals/mole deg.) can be used to obtain $\Delta G°_f/RT$ of Al_2O_3 liquid.

In the second part of this paper we wish to calculate the equilibration conditions in terms of pressure and temperature of a lava with a solid compound or with an assemblage of minerals. In Table 8 we have listed the relevant thermodynamic data for these solids, which in conjunction with the heat capacity equations of Kelley (1960) suffice for the calculations.

B. Application to Petrogenesis

A large amount of effort has been invested in the experimental exploration of basic liquids formed by partial fusion of garnet-lherzolite, eclogite, pyrolite and other model mantle materials. This type of investigation, with or without water as an additional component, has been summarized by Green (1970) who has shown on a P-T grid the conditions under which liquids, corresponding to almost all the principal lava types, could have been generated by partial fusion. This experimental approach is only of general utility as the results cannot be presently used to deduce the pressure-temperature conditions of equilibration of a particular lava with a particular source material.

In the second part of this paper we consider one of the petrological-thermodynamic approaches available to the individual investigator who wishes to calculate the P-T conditions of equilibration of any basic lava with any stipulated source material, and who additionally desires to obtain some information of the composition of the solid residue.

The generation, ascent, eruption and crystallisation of basic magma involves a sequence of time-dependent conditions which are difficult to quantify. Indeed the general petrological approach to this dynamic system is to identify various "static" stages in the evoluation of a basic magma, and assume that for a particular segment of the life-cycle of the magma, these conditions were typical of the whole. This difficulty can be illustrated by the crystallisation of a basic lava on the earth's surface. Among the minerals which precipitate are the iron-titanium oxides whose composition can be used to derive both the temperature and oxygen fugacity of their equilibration. This temperature is presumably the temperature at which the reaction rate effectively became zero, and this may, or may not, be the temperature at which the reaction rates for the coexisting minerals also became zero. At best it represents one point in the life cycle of the magma, and it is a petrological necessity to determine the properties of the coexisting minerals at this same point. Therefore we have to make the assumption that the iron-titanium oxide equilibration temperature, hereafter called the quench temperature for brevity, applied to the whole groundmass assemblage. General petrological experience would suggest that this is rarely the case, for some of the minerals are strongly zoned. Often, however, the average bulk composition of a particular mineral comes close to that found in slowly cooled intrusions.

Similarly the thermodynamic estimates of pressure and temperature made in the later part of this paper refer to a "static" segment in the life cycle, and thus in a dynamic magma regime to a smeared average of conditions which the techniques used here are unable yet to resolve further.

In what follows we, if effect, reverse the P-T path that a lava took in its ascent from source to surface, and in so doing we assume that the concentrations of all the components which determined the mineralogical composition of the lava as it crystallised on the surface remain unchanged in the inverse path to the source. In many lavas this assumption may be difficult to sustain, but in those alkali-olivine-basalt lavas which bring up ultrabasic mantle fragments (ρ = 3.3-3.4) 2 cms or more in diameter (up to 150 cms have been recorded) crystal settling is obviously not an operational method of changing the composition of the lava for that segment of its ascent path since the fragments were included. Until more is known of the rates of ascent of all varieties of magma, other than alkali-basalts containing nodules, it is difficult to make any statement of the viability of crystal fractionation changing the composition of the liquid during its ascent.

TABLE 8

Heats of Formation ($\Delta H^\circ_{f,\,298}$), Entropies, S°_{298}, Volumes ($a_s T + b_s$)

and Compressibilities of Solid Compounds Used in Equilibration Calculations

Solid	$(\Delta H^\circ_f)_{298}$	S°_{298}	V(cal./bar) $a_s \times 10^6$	b_s	$\beta \times 10^6$
$MgAl_2O_4$ spinel	-551200	19.27	26.04	0.9408	0.41
$CaAl_2Si_2O_8$ anorthite	-1009300	48.45	-	-	-
$NaAlSi_2O_6$ jadeite	-719871	31.90	38.75	1.4314	0.75
Mg_2SiO_4 forsterite	-520300	22.75	35.78	1.0349	0.79
$MgSiO_3$ orthoenstatite	-370200	16.20	22.54	0.7444	1.01
$FeTiO_3$ ilmenite	-295560	25.30	-	-	-
Fe_2TiO_4 ulvospinel	-360992	40.36	61.51	1.1184	0.5
$CaMgSi_2O_6$ diopside	-765100	34.20	46.27	1.5644	1.07
$KAlSiO_4$ kaliophilite	-503926	31.85	86.72	1.4356	2.05
$KAlSi_3O_8$ sanidine	-944378	56.94	70.94	2.5795	1.76
$Ca_3Al_2Si_3O_{12}$ grossular	-1588393	57.70	70.46	2.9725	0.60
Ca_2SiO_4 calcium-olivine	-553973	28.80	-	-	-
SiO_2* β-quartz	-217725	9.00	-3.82	0.5703	1.776
SiO_2 glass	-215870	11.33	1.0559	0.6515	2.3
$CaAl_2SiO_6$ pyroxene	-786984	34.60	-	-	-
$KMg_3AlSi_3O_{10}(OH)_2$ hydroxy phlogopite	-1492800	76.40	117.69	3.5490	2.34

*Metastable at 298.15; extrapolated down to 298.15 from α-β transition.

Some recent results on the heats of solution of enstatite, forsterite and quartz (Charlu et al., 1975) indicate substantial differences for $\Delta H^\circ_{f,298}$ to those listed above, in particular for enstatite. However this new data shows that forsterite and β-quartz, and forsterite and cristobalite, would be stable above about 1060°C. As this is most unlikely, we have retained the older data for enstatite which is more compatible with the known instability of quartz and forsterite.

Data taken from Robie and Waldbaum (1968), Pankratz (1968), JANAF (1971) Helgeson (personal communication, 1974), Verhoogen (1962), Skinner (1966), Birch (1966), Robie et al. (1967).

The volatile components, particularly H_2O, CO_2 and SO_2 would be expelled as the lava erupted and crystallised on the earth's surface. Initially we will ignore any increase in the concentration of water in the inverse path, but later we relax this constraint and consider the effect of variable water concentration as far as the experimental and thermodynamic data will allow.

This second part will consider several topics: (i) a thermodynamic approach to the calculation of the P-T equilibration of a basic lava with any stipulated source material, (ii) the thermal response of magma to engulfing cooler ultrabasic nodules, and (iii) the concentration of water in lavas; we defer to the third part heat and mass transfer rates for ascending basaltic magma.

The thermodynamic treatment here is substantially that of Nicholls and Carmichael (1972), except that the assumptions of that paper are tested here against experimental liquid-solid equilibria, and are also modified to consider more complicated components than simple oxides.

At equilibrium at some pressure and temperature between a silicate liquid and crystals we may write

$$\underline{\mu}_i^{liq} = \underline{\mu}_i^{solid} \qquad (4)$$

where i is a component in the superscript phase. There is no theoretical restriction to the components that may be chosen, except that $\sum_i X_i = 1$ where X_i is the mole fraction of i. In practice it is difficult either to define the activities

of many components in a lava, or obtain thermodynamic data for the chosen components. In this paper we use liquid $NaAlSi_3O_8$, $KAlSi_3O_8$, $CaMgSi_2O_6$, Fe_2SiO_4, Al_2O_3, TiO_2 but SiO_2 glass for which the standard state thermodynamic data have been given earlier (Table 7).

It is convenient to consider the lava (the equivalent liquid) first, as the relationships here are more complicated, and involve several digressions into the thermodynamic treatment of solutions.

The Lava and Activities at 1 bar

Basic lavas are quenched on the surface of the earth (P = 1 bar) to an assemblage of minerals which typically include plagioclase, calcium-rich pyroxene, olivine, iron-titanium oxides and sometimes a calcium-poor pyroxene. If the temperature of the lava can be obtained, most conveniently from the composition of the coexisting iron-titanium oxides using the calibration curves of Buddington and Lindsley (1964), then with analyses of the groundmass minerals, the activities of several components can be calculated at the quench temperature. With an assemblage of olivine and magnetite solid solutions $a^{lava}_{SiO_2}$ can be calculated from the reaction

$$\underset{\text{solid}}{\tfrac{2}{3}Fe_3O_4} + \underset{\text{glass}}{SiO_2} = \underset{\text{solid}}{Fe_2SiO_4} + \underset{\text{gas}}{\tfrac{1}{3}O_2} \qquad (5)$$

which gives

$$\ln a^{lava}_{SiO_2} = \Delta G^{\circ}_5/RT + \ln a^{olivine}_{Fe_2SiO_4} + \tfrac{1}{3}\ln f_{O_2} - \tfrac{2}{3}\ln a^{magnetite}_{Fe_3O_4}$$

for which over the temperature range 900-1300 K (Wones and Gilbert, 1969)

$$\Delta G^{\circ}_5/RT = 19042/T - 6.47$$

and the method of treating the activity-composition relations of the solids will be considered in detail below.

The general form of $\Delta G^{\circ}/RT$ is given by

$$\frac{\Delta G^{\circ}}{RT} = [-a(\ln T - 1) - \frac{1}{2}bT + (\Delta H_{Tr} - aTr + cTr^{-1} - b/2\ Tr^2)T^{-1} - \frac{c}{2}T^{-2} + (-\Delta S_{Tr} + a\ln T_r + bTr - \frac{c}{2}Tr^{-2})]\ 1/R$$

where ΔH_{Tr}, ΔS_{Tr} represent the standard state enthalpy and entropy change at a reference temperature Tr, and a, b, c are the coefficients of the Maier-Kelley heat capacity equation of the products less the reactants. We have given in Table 9 the values of $\Delta G^{\circ}/RT$ for other reactions to calculate the activity of a component on a liquid standard state.

In what follows we have used the superscript lava to denote conditions at 1 bar and the quench temperature, whereas the superscript liquid is used to refer to conditions at elevated P and T.

Activity-Composition Relations; Solid Solutions

It is often convenient, for petrological purposes, to assume that all but one of the solid solutions used to define the activity of a particular component are ideal, especially over small composition ranges, and so let any actual departure from ideality of these become incorporated in the activity coefficient of the one designated solid solution. The standard state free-energy change of reaction 5 has been experimentally determined by Wones and Gilbert (1969), and so far as possible all the derived activity coefficients used in this paper are made internally consistent with this reaction.*

From reaction 5 it is apparent that for any lava which contains olivine, magnetite solid solution and quartz, which precipitated at a known pressure, temperature and oxygen fugacity, the latter two variables being obtained from the iron-titanium oxides (Buddington and Lindsley, op. cit.) it is possible to calculate the activity of Fe_3O_4 in the magnetite solid solution. However the value obtained will depend on the mixing model used for olivine solid-solution series. For the Fe-Mg olivine series Williams (1972) found small departures from ideality, but we have noted that the difference between the activity of Fe_2SiO_4 calculated according to his model, and that calculated on the assumption of ideal two-site mixing ($a_{Fe_2SiO_4} = X^2_{Fe_2SiO_4}$) (Kerrick and Darken, 1975) often lies well within the uncertainty of estimating the composition of a compositionally zoned olivine in a lava. Thus we have assumed that the Fe-Mg olivines mix ideally, and therefore that the activity coefficient of either Fe_2SiO_4 or Mg_2SiO_4 is not a function of olivine composition.

Treating the mixing of Fe_3O_4 in a titanomagnetic solid solution is more complicated, as Fe_2TiO_4, Fe_3O_4 and $MgFe_2O_4$ are inverse spinels e.g., $Fe^{3+}_{oct}(Fe^{2+}Fe^{3+})O^{\overline{\ }}_{tet}$ while some of the other (dilute) components, such as $MgAl_2O_4$ are not. As there is no unambiguous method of recalculating a microprobe analysis of a titanomagnetite solid solution, and thus of assigning atoms to either the tetrahedral or octahedral sites, it is necessary to assume that $a_{Fe_3O_4} = X_{Fe_3O_4}$. It has been demonstrated that within the limits of error of the standard state thermodynamic data, $\gamma_{Fe_3O_4}$ is unity in the temperature range 835-1035°C, and in the composition range 0.425-0.226 Fe_3TiO_4, for naturally occurring titanomagentite (Heming and Carmichael, 1973). Moreover Nicholls et al. (1971) were able to show a parallel internal consistency of thermodynamic data based on this assumption for a ugandite lava, where $a^{lava}_{SiO_2}$ could be calculated both from reaction 5 and from the coexistence of kalsilite and leucite.

*Their mineral assemblage contained solid SiO_2 as the standard state of SiO_2, so that their measured values have been changed to a standard state of SiO_2 glass.

TABLE 9

Reactions which Define the Activity of a Component in the Lava and the Constants in the Expression for the Standard State Free Energy Change of the Reaction:

$\Delta G^\circ/RT = A\ (\ln T - 1) + BT + C^{-1} + DT^{-2} + E$

Reaction No.	Reaction	A	B 10^3	C	D 10^{-5}	E
6	Fe_2SiO_4 liquid $\rightleftarrows$ Fe_2SiO_4 solid	10.462	-2.335	-952.412	1.690	-61.9063
7	$CaMgSi_2O_6$ liquid $\rightleftarrows$ $CaMgSi_2O_6$ solid	14.920	0.6617	10562.0	3.960	-103.3363
8	$NaAlSi_3O_8$ liquid $\rightleftarrows$ $NaAlSi_3O_8$ solid	12.072	-3.497	1301.12	3.777	-71.5698
9	$KAlSi_3O_8$ liquid $\rightleftarrows$ $KAlSi_3O_8$ sanidine	9.928	-3.246	-35.2072	4.290	-57.8935
10	$CaMgSi_2O_6$ + Al_2O_3 + $1/2SiO_2$ $\rightleftarrows$ solid liquid glass					
	$CaAl_2Si_2O_8$ + $\frac{1}{2}Mg_2SiO_4$ solid solid	8.834	-1.834	339.197	0.9272	-59.5084
11	TiO_2 + Fe_2TiO_4 $\rightleftarrows$ $2FeTiO_3$ liquid solid solid	2.184	1.2857	-560.7506	1.5549	-16.6055
12	TiO_2 + $1/2\ Fe_2SiO_4$ $\rightleftarrows$ $FeTiO_3$ liquid solid solid	5.2511	-0.697	2399.8	0.7963	-35.2616
	+ $1/2\ SiO_2$ glass					
13	TiO_2 + Fe_2SiO_4 $\rightleftarrows$ Fe_2TiO_4 liquid solid solid	8.318	-2.680	5360.4	0.377	-53.9176
	+ SiO_2 glass					

In the pyroxenes there are two octahedral cation sites, an m2 site and a smaller m1 site together with the tetrahedral t sites. The activity can be written as

$$a^{\text{pyroxene}}_{CaMgSi_2O_6} = (X_{Ca}\gamma_{Ca})_{m2}\ (X_{Mg}\gamma_{Mg})_{m1}\ (X_{Si}\gamma_{Si})^2_t$$

and we have assumed $\gamma_{Ca}\gamma_{Mg}\gamma^2_{Si} = 1$

where $X_{Ca} = n_{Ca}/(n_{Ca} + n_{Mn} + n_{Na} + n_{Mg^1} + n_{Fe^1})$

$$X_{Mg} = n_{Mg}/n_{Mg^1} + n_{Fe^1} + n_{Al} + n_{Ti} + n_{Cr})$$

$$X_{Si} = n_{Si}/(n_{Si} + n_{Al})$$

where n_{Ca} etc. is the number of atoms in the 6 oxygen pyroxene formula; note that n_{Mg^1} and n_{Fe^1} represent the amount of Mg and Fe required to balance the number of cations in the m1 and m2 sites, and they are allotted in proportion to the Fe/Mg ratio of the pyroxene.

Similar reasoning and assumptions would give for orthopyroxene

$$a^{\text{orthopyroxene}}_{MgSiO_3} = [(X_{Mg})_{m2}\ (X_{Mg})_{m1}\ (X^2_{Si})_t]^{\frac{1}{2}}$$

so that for typical aluminous orthopyroxenes of Mg/Mg + Fe $\simeq$ 0.88, the calculated $a_{MgSiO_3} \simeq 0.73$.

The interpretation of the experimental results on the mixing of the Fe-Mg pyroxenes is conflicting. Navrotsky (1971) has concluded that the orthopyroxenes are essentially ideal at temperatures above 1000°C; Nafziger (1973) came to essentially the same conclusion for monoclinic pyroxenes in equilibrium with spinels. However Williams (1971), dealing with much the same temperature range as Nafziger, optically identified his pyroxenes as orthorhombic on the basis of their straight extinction, and used a regular solution mixing model to represent their departure from ideality. Wood and Strens (1971) have used the two-site mixing model for orthopyroxene, and their calculated Fe/Mg ratio for pyroxenes in equilibrium with olivine agrees closely with the experimental results of Smith (1970).

An ideal multi-site mixing model is used for spinel in the source region, namely

$$a^{\text{spinel}}_{MgAl_2O_4} = (X_{Mg}\gamma_{Mg})(X^2_{Al}\gamma_{Al}) \text{ where } \gamma_{Mg}\gamma_{Al} = 1$$

for these spinels contain only small amounts of spinel components with inverse structures, so that the activity of $MgAl_2O_4$ may be approximated by ideal ionic mixing in the octahedral and tetrahedral sites. For grossular garnet we have used the activity coefficient determined by Hensen et al. (1975) and we have also assumed ideal mixing of $NaAlSi_3O_8$ and $CaAlSi_2O_8$ in high temperature plagioclase.

Henceforth we use these activity-composition relationships consistently throughout the remainder of this paper, noting that as we are calculating $a_{CaMgSi_2O_6}$ in the lava from the activity of $CaMgSi_2O_6$ in the groundmass augite, and later considering the equilibration of the lava with an augite in the mantle, then provided that we formulate the activity of $CaMgSi_2O_6$ in the same way for both, any errors will tend to cancel.

Values of $RT\ell n\gamma^{pyroxene}_{NaAlSi_2O_6}$ and $RT\ell n\gamma^{pyroxene}_{CaAl_2SiO_6}$

In basic lavas which contain a groundmass assemblage of plagioclase, olivine, calcium-rich pyroxene and iron-titanium oxides, the following reaction may be used to obtain the activity coefficient of $NaAlSi_2O_6$ in the augite pyroxene,

$$NaAlSi_2O_6 + SiO_2 = NaAlSi_3O_8$$

solid glass solid

If the ideal contribution to the activity of $NaAlSi_2O_6$(jd) in the pyroxene is expressed as

$$\hat{X}_{jd} = (X_{Na})_{m2}(X_{Al})_{ml}(X^2_{Si})_t$$

then by using the temperature obtained from the coexisting iron-titanium oxides, and the activity of SiO_2 calculated from reaction 5, the activity coefficient of jadeite can be calculated. Note that any errors in the standard state thermodynamic data, or in the assumption of ideal mixing in the feldspar are incorporated in this activity coefficient. As an example, we have set down the pertinent information for a basanite lava (Bacon and Carmichael, 1973)

	T°K	$X^{plagioclase}_{NaAlSi_3O_8}$	$\ell n\, a^{lava}_{SiO_2}$	$\hat{X}_{jd}$	$RT\ell n\gamma_{jd}$
CSQ-3	1278	.443	-1.9844	1.851×10^{-3}	5020 cal

The average value of $RT\ell n\gamma_{jd}$ calculated from ten lavas, spanning the composition range of high alumina basalts, tholeiites and basanites, and the temperature range 1253-1353K, is

$$RT\ell n\gamma_{jd} = 5580 \text{ cals. with a standard deviation of 1820 cals.}$$

Much of the error will reside in the microprobe analysis of Na_2O in the pyroxene. Ganguly (1973) has shown that jadeite-diopside compositions are virtually ideal above 1100°C, but below this temperature there is not ideal mixing, and he represented the low temperature mixing by a quadratic solution model (Rowlinson, 1969).

Approximating the pyroxene solution as a binary between jadeite and "others" the activity coefficient of jadeite becomes:

$$\ell n\, \gamma_{jd} = W(1 - \hat{X}_{jd})^2/RT$$

for the quadratic model. In the limit as $X_{jd} \to 0$ (i.e. in the range appropriate for an infinite dilution approximation) we have

$$RT\ \ell n\ \gamma_{jd} = W \quad \text{(a constant)}$$

in agreement with the formulation given above.

A similar approach on the same lavas has been used to determine $\gamma_{CaAl_2SiO_6}$ using the reaction

$$CaAl_2SiO_6 + SiO_2 = CaAl_2Si_2O_8 \qquad (15)$$

solid glass solid

If the ideal contribution to the activity of $CaAl_2SiO_6$ (cats) is expressed as

$$\hat{X}_{cats} = (X_{Ca})_{m2}(X_{Al})_{ml}{}^4(X_{Al}\cdot X_{Si})_t$$

then

$$\ell n\gamma^{pyx}_{cats} = \Delta G°/RT + \ell n\, a^{plagioclase}_{CaAl_2Si_2O_8} - \ell n\, X^{pyx}_{cats} - \ell n\, a^{lava}_{SiO_2}$$

and the average value of $RT\ell n\gamma^{pyx}_{cats}$ for the same ten lavas is

$$RT\ell n\gamma^{pyx}_{cats} = 6700 \text{ cals with a standard deviation of 1730 cals.}$$

Calculation of $RT\ell n\gamma^{olivine}_{Ca_2SiO_4}$

Stormer (1973) has shown that the calcium content of olivine in a magma is a function of silica activity, temperature and pressure, and it is appropriate to calculate the activity coefficient of Ca_2SiO_4 in groundmass olivine (1 bar) for lavas which have crystallized at known temperatures. By representing the mineralogical assemblage as

$$\tfrac{1}{2}Ca_2SiO_4 + \tfrac{1}{2}Mg_2SiO_4 + Fe_2SiO_4 + \tfrac{1}{3}O_2$$

ca-olivine forsterite fayalite gas

$$= CaMgSi_2O_6 + \tfrac{2}{3}Fe_3O_4 \qquad (16)$$

diopside magnetite

for which $\Delta G°_{16}/RT = -25223/T + 7.967$ in the temperature range 1100-1500K. By re-arrangement

$$\ell n\, a_{Ca_2SiO_4} = \Delta G°_{16}/RT + \ell n\, \frac{a^{pyroxene}_{CaMgSi_2O_6}\cdot (a^{titanomagnetite}_{Fe_3O_4})^{\frac{2}{3}}}{(a^{olivine}_{Mg_2SiO_4})^{\frac{1}{2}}\cdot a^{olivine}_{Fe_2SiO_4}\cdot f_{O_2}^{\frac{1}{3}}}$$

and as

$$a_{Ca_2SiO_4} = X^2_{Ca_2SiO_4}\cdot \gamma^2_{Ca_2SiO_4}$$

then

$$\tfrac{1}{2}RT\ \ell n\ a_{Ca_2SiO_4} = RT\ \ell n\ X^{olivine}_{Ca_2SiO_4} + RT\ \ell n\ \gamma_{Ca_2SiO_4}$$

and $RT\ \ell n\ \gamma_{Ca_2SiO_4}$ for nine lavas, basanites and tholeiites, is plotted as a function of olivine composition in Figure 6. Although there is some scatter, presumably arising form errors in both

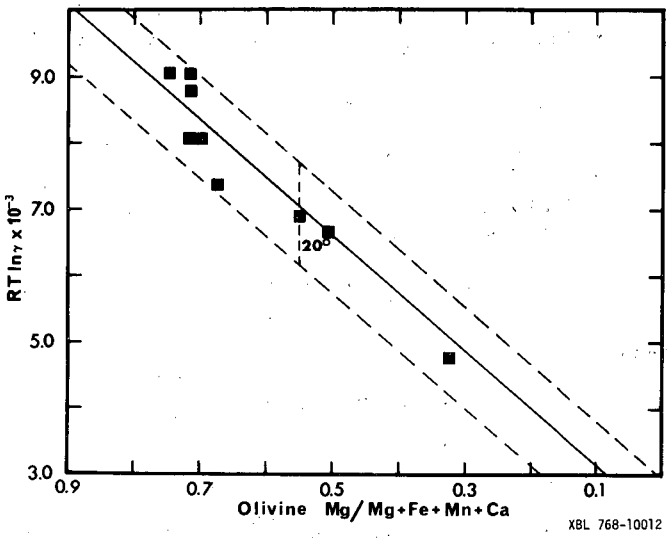

Fig. 6. Plot of $RT\ell n\gamma^{olivine}_{Ca_2SiO_4}$ at 1 bar against olivine composition using analyses of groundmass olivine in a variety of basalts. The limits of 20° variation in temperature are shown for one point. The equation of the least squares line is given in the text.

temperature and Ca determinations, the line of best fit is

$$RT\ \ell n\gamma_{Ca_2SiO_4} = 8651X_{Mg} + 2286 \quad (17)$$

with a correlation coefficient of 0.92.

This line is in accord with regular solution theory, for in a ternary regular solution of Ca_2SiO_4, Fe_2SiO_4 and Mg_2SiO_4 (Prigogine and Defay, p. 257; 1954)

$$RT\ \ell n\gamma_{Ca_2SiO_4} = (X_{Fe_2SiO_4})^2\ W_{Fe-Ca} + (X_{Mg_2SiO_4})^2\ W_{Mg-Ca} + (X_{Fe_2SiO_4} \cdot X_{Mg_2SiO_4})(W_{Fe-Ca} - W_{Fe-Mg} + W_{Mg-Ca}) \quad (18)$$

where W represents the interaction between the subscript components, and is a constant for each interaction. If Mg-Fe exchange in olivines is assumed to be ideal, then $W_{Fe-Mg} = 0$, and since the amount of Ca_2SiO_4 in these olivines is small ($X_{Ca_2SiO_4} = .0051 - .0092$), they can be considered as a binary Fe-Mg solid solution. Thus

$$X_{Fe_2SiO_4} = (1 - X_{Mg_2SiO_4}) \quad (19)$$

and by substituting equation 19 into equation 18 we find that

$$RT\ \ell n\ \gamma_{Ca_2SiO_4} = X_{Fe_2SiO_4} \cdot W_{Fe-Ca} + X_{Mg_2SiO_4} \cdot W_{Mg-Ca}$$

which is a straight line in agreement with the results in Figure 6.

With a knowledge of $RT\ \ell n\gamma_{Ca_2SiO_4}$, the activity of silica can be calculated in those lavas without iron-titanium oxides, and without other combinations of phases to define silica activity. The appropriate reaction is

$$\tfrac{1}{2}Ca_2SiO_4 + \tfrac{1}{2}Mg_2SiO_4 + SiO_2 = CaMgSi_2O_6 \quad (20)$$

Ca-olivine forsterite glass diopside

As the leucite-basanities from Vesuvius do not contain a groundmass mineral assemblage which conveniently define silica activity, the coexisting olivine and pyroxene using equation 20 and the appropriate value for $RT\ \ell n\ \gamma_{Ca_2SiO_4}$ from equation 17 can be used to calculate their activities of silica.

The discussion so far has treated the activity-composition relations of various solid solutions in a rather empirical way, either making plausible assumptions of ideal multi-site mixing, or obtaining activity coefficients from standard-state free energy data coupled with ideal mixing of the solid solution used to define the activity of the chosen component. For liquids the situation is more difficult, as there is far less experimental work to indicate the appropriate mixing model. For this reason the thermodynamics of solutions are considered in more detail, although they apply to all solutions, liquid or solid.

Activity-Composition Relations: Liquids

Before examining the pressure and temperature dependence of the activity coefficients in the liquid, so as to take account of both increasing pressure and temperature in the inverse path of the lava, it is necessary to digress into how γ_i is calculated given that a_i is known. This requires that the ideal contribution to the activity of i, $\hat{X}_i$, be known, or formulated.

Calculation of $\ell n\hat{X}_i^{liquid}$

In order to obtain a value for $\ell n\gamma_i^{liquid}$, given that

$$\ell n\gamma_i^{liquid} = \ell na_i^{liquid} - \ell n\hat{X}_i^{liquid}$$

some method must be found for calculating the ideal contribution to the activity of the multioxide compounds that we use here. It is clear that $\hat{X}_{SiO_2}$ and $\hat{X}_{Al_2O_3}$ could be represented by the mole fractions of the two oxides reported in the chemical analysis of the lava. However $\hat{X}_{CaMgSi_2O_6}$, the ideal contribution to the activity, is not so obviously calculated, and we have used the following method which has been borrowed from aqueous electrolyte chemistry (Klotz 1964, p. 391). Consider for example a pure $CaMgSi_2O_6$ liquid for which we may write

$$CaO + MgO + 2SiO_2 = CaMgSi_2O_6$$

liquid liquid liquid liquid

Since it is pure liquid, then $\hat{X}_{CaMgSi_2O_6} = 1$.

But we wish to use the simple liquid oxides as components so that we define

$$\hat{X}\ CaMgSi_2O_6 = 1 = (X^{liq}_{SiO_2})^2 X^{liq}_{CaO}\ X^{liq}_{MgO}\ \lambda^*$$

and thus

$$\hat{X}\ CaMgSi_2O_6 = (\tfrac{1}{2})^2 \cdot \frac{1}{4} \cdot \frac{1}{4}\ \lambda^* = 1$$

so that $\lambda^* = 64$ and λ^* is a factor which depends on stoichiometry and will make $\hat{X} = 1$ for the pure liquid compound. Similar reasoning gives for:

$$\hat{X}^{liquid}_{Fe_2SiO_4} = \lambda^* \left[\left(X^{liq.}_{FeO}\right)^2 X^{liq.}_{SiO_2}\right] \text{ where } \lambda^* = 6.75$$

$$\hat{X}^{liquid}_{NaAlSi_3O_8} = \lambda^* \left[\left(X^{liq.}_{Na_2O}\right)^{\frac{1}{2}} \left(X^{liq.}_{Al_2O_3}\right)^{\frac{1}{2}} \left(X^{liq.}_{SiO_2}\right)^3\right]$$

where $\lambda^* = 18.963$

The Pressure and Temperature Dependence of Activity Coefficients

Although experiments can be devised to determine the temperature dependence of the Gibbs free-energy of a multi-component silicate liquid, natural silicate liquids have such a large range of composition that the experimental effort required would be enormous. It is far more practical at this stage to thermodynamically model the temperature dependence of the activity coefficients, which are related to the Gibbs free energy of the solution by

$$G = \sum_i n_i \underline{\mu}_i$$

from which the excess Gibbs free energy (G^{xs}) is given by the relation $G = G^\circ + G^{ideal} + G^{xs}$ and so

$$dG^{xs} = RT \sum_i n_i d\ell n\ \underline{\gamma}_i + RT \sum_i \ell n \underline{\gamma}_i dn_i$$

so that under the stated constraints, the first term on the right is zero as required by the Gibbs-Duhem equation, and

$$(\partial G^{xs}/\partial n_i)_{T,P,nj} = \underline{\mu}^{xs}_i = RT\ell n\underline{\gamma}_i$$

For the partial molar quantities, we have

$$\bar{V}_i = V^\circ_i + RT\ (\partial \ell n \underline{\gamma}_i/\partial P)_{T,nj} \qquad (21)$$

$$\bar{S}_i = S^\circ_i - R\ell n a_i - RT(\partial \ell n \underline{\gamma}_i/\partial T)_{P,nj} \qquad (22)$$

$$\bar{H}_i = H^\circ_i - RT^2(\partial \ell n \underline{\gamma}_i/\partial T)_{P,nj} \qquad (23)$$

$$\bar{C}p_i = Cp^\circ_i - 2RT(\partial \ell n \underline{\gamma}_i/\partial T)_{P,nj} - RT^2(\partial^2 \ell n \underline{\gamma}_i/\partial T^2)_{P,nj} \qquad (24)$$

and the excess partial functions can be obtained by subtraction of the ideal quantities.

It has been shown above that the activity relative to a liquid standard state of several components in the lava can be calculated from the composition of the solid assemblage. It is now necessary to determine how these liquid activity coefficients change with P and T in the absence of solids, as the original P-T path of the magma from its source is inverted. The liquid is assumed to be of constant composition for reasons discussed in the beginning of this paper.

The Pressure Dependence of γ_i

From equation 21, the pressure dependence of γ_i can be obtained if the values of $\bar{V}_i$ and V°_i are known as a function of pressure and temperature. The partial molar volumes, $\bar{V}_i$ for several oxide components in silicate liquids at 1 bar have been calculated by Bottinga and Weill (1970); a least squares fit to their data are given in Table 10. As there is no simple way to define the properties of a stoichiometric compound when it is dissolved in a non-stoichiometric liquid, we have assumed that, for example $\bar{V}_{Fe_2SiO_4} = 2\bar{V}_{FeO} + \bar{V}_{SiO_2}$ and $\bar{V}_{NaAlSi_3O_8} = \frac{1}{2}\bar{V}_{Na_2O} + \frac{1}{2}\bar{V}_{Al_2O_3} + 3\bar{V}_{SiO_2}$.

TABLE 10

Least squared values of $\bar{V}$ after Bottinga and Weill (1970). Also shown are $\bar{V} - V^\circ$ for the liquid compounds used in this paper. Units of cal bar^{-1}.

	$\bar{a}_L \times 10^6$	$\bar{b}_L$
SiO_2	6.15	0.6304
TiO_2	64.65	0.3937
Al_2O_3	24.37	0.8664
FeO	47.80	0.2259
MgO	64.65	0.1683
CaO	71.70	0.2744
Na_2O	164.33	0.4157
K_2O	329.51	0.5482

$\bar{V} - V^\circ$ in the form of $aT + b + cP + dPT$

	$a^\circ_L \times 10^6$	b°_L	$c^\circ_L \times 10^6$	$d^\circ_L \times 10^{12}$
SiO_2	5.09	-.02110	-1.162	2.429
Fe_2SiO_4	0.0	0.0	0.0	0.0
$KAlSi_3O_8$	117.36	-.1457	0.0	0.0
$NaAlSi_3O_8$	-59.10	0.1595	0.0	0.0
$CaMgSi_2O_6$	-29.60	0.0952	0.0	0.0
TiO_2	8.68	0.0050	0.0	0.0
Al_2O_3	-306.62	0.8265	0.0	0.0

As we have expressed the variation of the volume of the liquid compounds (Table 7) as

$$V^\circ = a^\circ_L T + b^\circ_L + c^\circ_L P$$

then subtraction of this expression from $\bar{V}$ gives $\bar{V} - V^\circ$. Thus

$$\bar{V} - V^\circ = (\bar{a}_L - a^\circ_L) T + (\bar{b}_L - b^\circ_L) + (\bar{c}_L - c^\circ_L) P$$

but as there are no data available on $\bar{c}_L$, we have assumed that $\bar{c}_L = c^\circ_L$ or in other words that $\bar{V} - V^\circ$ is independent of pressure. Only for SiO_2 is this not the case, for V° refers to the standard state of SiO_2 glass, whereas $\bar{V}$ refers to SiO_2 in the liquid solution. It is well known that β for liquids is greater than for the corresponding glasses and we have used the value $(\bar{c}_L)_{SiO_2} = (\partial\bar{V}/\partial P)_T = -2.66 \times 10^{-6}$ which is the mean value of the extrapolation of the compressibility of Na_2O-SiO_2 and K_2O-SiO_2 liquids (Janz, 1967) to pure SiO_2.

Thus with the exception of SiO_2, the integration of $\bar{V} - V^\circ$ in equation 21 can be assumed to be independent of pressure, so that between the limits of 1 and P bars

$$(\ell n\ \underline{a}_i^{liq})_T^P = (\ell n\ \underline{a}_i^{lava})_T^{1\ bar} + \frac{\bar{V} - V^\circ}{RT}(P-1) \qquad (25)$$

The Temperature Dependence of γ_i

There are few data on multicomponent silicate liquids, corresponding to lavas, to indicate the form of the temperature dependence of γ_i, although Burnham (1975) has suggested that with the appropriate choice of components, signifying polmerisation of SiO_2 and $NaAlSi_3O_8$, natural silicate liquids saturated with H_2O, may mix ideally ($\gamma = 1$), a conclusion also reached by Flood and Knapp (1968) for anhydrous binary systems of SiO_2 and the feldspar components. Until vapor pressure measurements have been made of the components in equilibrium with silicate liquids, it is not possible to predict what polymer arrangements are present in multicomponent silicate liquids, and no consistent group of polymeric components can yet be chosen that will allow their activity coefficients to become unity. As the data to support any chosen mixing model are sparse, a simple model has obvious advantages, provided that it can reproduce liquid-solid phase equilibria.

One such is the quadratic solution model (Rowlinson, 1969) and in a binary system, the excess free-energy of this solution is given by

$$G^{xs} = X_1 X_2 W$$

which satisfies the requirement that G^{xs} should be zero for pure X_i or X_2. By differentiation

$$\left(\frac{\partial G^{xs}}{\partial n_i}\right)_{\rho,T,nj} = \underline{\mu}_i^{xs} = (1 - x_i)^2 W \qquad (26)$$

so that

$$\underline{\mu}_i = \underline{\mu}_i^\circ + RT\ \ell n\ x_i + (1 - x_i)^2\ W \qquad (27)$$

or

$$\ell n\ \underline{a}_i = \ell n\ x_i + \frac{(1-x_i)^2 W}{RT}$$

where W is called an interaction parameter, with units of cals. $mole^{-1}$. From equation 26 we obtain

$$\left(\frac{\partial \mu^{xs}}{\partial T}\right)_{P,nj} = (1 - x_i)^2 \left(\frac{\partial W}{\partial T}\right)_{P,nj} = -\bar{S}_i^{xs} \qquad (28)$$

and

$$T\left(\frac{\partial \bar{S}_i^{xs}}{\partial T}\right)_{P,nj} = -T(1 - x_i)^2 \left(\frac{\partial^2 W}{\partial T^2}\right)_{P,nj} = \bar{C}_{P_i}^{xs} \qquad (29)$$

If $(\partial W/\partial T)_P$ is zero, then a quadratic solution is called a regular solution, which has therefore as its necessary conditions that $(\partial RT\ \ell n\ \gamma_i/\partial T)_P = 0$ (equation 22) and $C_P^{xs} = 0$ which has been established in the first part of this paper.

Several investigators have shown that a regular solution model will account for the observed behavior of the activity coefficient in silicate liquids; thus Lumsden (1961) was able to treat the liquids of the system FeO-Fe_2O_3 - SiO_2, over a temperature range of 200°C, as a ternary regular solution, Somerville et al. (1973) similarly modelled liquids of the four component system $FeO + MnO + AlO_{1.5} + SiO_2$ at 1550°C, and Nicholls and Carmichael (1972) showed the liquids saturated with corundum in the system Na_2O - Al_2O_3 - SiO_2 behaved as regular solutions.

The approach taken in this paper also uses the regular solution model for lavas, following the lead of Kudo and Weill (1970), but with the added restriction that the composition of the lava remains constant. Nicholls and Carmichael (op. cit.) used the following formulation

$$\ell n\ \underline{a}_i = \ell n\ X_i + \frac{\phi_i}{T} \qquad (30)$$

so that from equation 27

$$\frac{\phi_i}{T} = \frac{(1 - X_i)^2 W}{RT} = \ell n\ \gamma_i \qquad (31)$$

for a binary solution; note that for a liquid of constant composition $(1 - X_i)^2 W/R$ is a constant.

By combining equation 30 with equation 25 we obtain the following

$$\left(\ell n\ \underline{a}_i^{liq}\right)^{P,T} = \ell n\ X_i + \frac{\phi_i}{T} + \frac{\bar{V} - V^\circ}{RT}(P - 1) \qquad (32)$$

which gives the temperature and pressure dependence of the activity of i in a liquid of constant composition.

If instead of treating equilibrium between a pure liquid and a pure solid compound as in equation 3, we retain the ℓn K term to account for both liquid and solid solutions, we have

$$(\ell n\ a_i^{liq})^{P,T} = \frac{1}{RT}\left\{ \Delta H_{Tr} + \int_{Tr}^{T}(Cp_{solid} - Cp_{liq})dT \right.$$
$$-T\left[\Delta S_{Tr} + \int_{Tr}^{T}\frac{Cp_{solid}}{T} - \frac{Cp_{liq}}{T}\ dT\right]$$
$$\left. + \int_{1}^{P}(V_{solid} - V_{liq})dP + RT\ \ell n a_i^{solid}\right\}$$

If this equation is now combined with equation 32, we obtain

$$\ell n X_i + \phi_i/T + \bar{V}_i - V_i^{\circ}(P-1)/RT$$
$$= \left[\Delta H^{\circ}_{Tr} + \int_{Tr}^{T}\Delta Cp^{\circ}dT - T\left(\Delta S^{\circ}_{Tr} + \int_{Tr}^{T}\frac{\Delta Cp dT}{T}\right)\right.$$
$$\left. + \int_{1}^{P}\Delta V^{\circ}dP + RT\ \ell n \Pi a_i^{solid}\right]\frac{1}{RT} \qquad (33)$$

in which the left hand side gives the variation of $\ell n\ a_i$ with P and T in the silicate liquid equivalent to the lava, and the right hand side incorporates a term ($RT\ \ell n\ \Pi a_i^{solid}$) for the composition of the single solid, or an assemblage of solids, which define the activity of i at P and T. In the integration of the standard state volume change of the reaction, both the thermal expansion, or rather dV/dT (Table 8) and compressibility are included, and are both assumed to be independent of temperature and pressure respectively. Equation 33 is the general equation used in this paper to calculate the condition of equilibration of a liquid with a solid, and is solved on a computer for P as a function of T.

The Regular Solution Formulation Applied to Experimental Equilibria

By using ϕ_i, calculated at 1 bar* and the lava quench temperature, the P-T conditions of equilibration of a lava with olivine, or any other phase, may be compared to experimental results. Those of Bultitude and Green (1971) are used here, as these authors provide considerable information on the composition of the solids in equilibrium with liquid, and of their experimental compositions, the picrite-nephelinite has the most abundant information on olivine. On the assumption that the liquidus of this lava at 1 bar is 1400°C, and the composition of the olivine Fa_{10}, then the calculated P-T curves of equilibration with olivine of varied composition are shown in Figure 7.

If in addition to the results shown in Figure 7, the remainder of Bultitude and Green's experiments are used, we find that the average difference between observed and calculated conditions for 27 data points for olivine and liquid is 0.84% Fe_2SiO_4 in the composition of the olivine, 29.8° in temperature and 5.7 kbar in pressure. For 5 data points involving augite and liquid, the average difference between observed and calculated conditions is 0.003

*The procedure to do this has been set out in detail by Nicholls and Carmichael (1972) and by Carmichael et al. 1974 (pp. 111-118) and thus need not be repeated here.

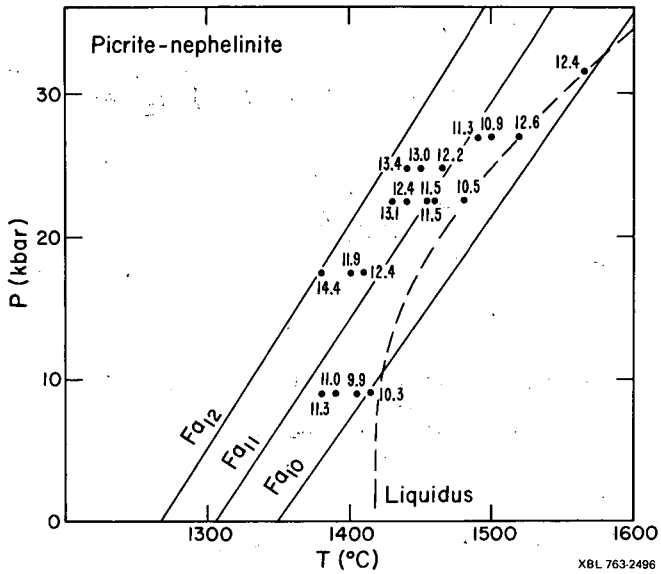

Fig. 7. Compositions of near liquidus olivine (crosses) given as %Fa for a picritic-nephelinite (Bultitude and Green, 1971) The calculated lines of equilibration of this lava with various olivine compositions are shown. The liquidus of this lava is also shown.

in the mole fraction of $CaMgSi_2O_6$ in the augite, 29° in temperature and 3.0 kbars in pressure. These errors are believed to be typical of using a regular solution model for the calculation of P-T equilibration conditions, but of necessity we have ignored any errors in composition, temperature and pressure in Bultitude and Green's results.

Equilibration of Basic Lavas with Stipulated Source Material

The composition of the solid residue with which we calculate the equilibration conditions of various lava types is

augite ($a_{CaMgSi_2O_6} = 0.4$; $\hat{X}_{NaAlSi_2O_6} = 0.03$)

spinel ($a_{MgAl_2O_4} = 0.614$) olivine ($X_{Mg_2SiO_4} = 0.90$)

garnet ($X_{Ca_3Al_2Si_3O_{12}} = 0.18$) opx ($a_{MgSiO_3} = 0.73$)

These minerals represent a typical solid residue judging from the composition of lherzolite nodules and relevant experimental equilibria (Aoki and Shiba, 1973; Boyd, 1969; Binns et al., 1970; Bacon and Carmichael, 1973; Green, 1973a).

By using reactions 6 and 7 (Table 8) for Fe_2SiO_4 and $CaMgSi_2O_6$ put in the form of equation 33, P-T lines of equilibration of the lava with the stated mineral compositions can be obtained. In addition, the activities of the SiO_2 and Al_2O_3 components will be defined in the solid residue by

$$Mg_2SiO_4 + SiO_2 = 2MgSiO_3 \qquad (34)$$

forsterite glass orthoenstatite

and then at P and T

$$\left(\ell n\ a^{liquid}_{SiO_2}\right)^{P,T} = \Delta G^{\circ}_{34}/RT + \int_1^P \frac{\Delta V^{\circ}}{RT}\, dP$$

$$+ \ell n\ \frac{\left(a^{pyroxene}_{MgSiO_3}\right)^2}{a^{olivine}_{Mg_2SiO_4}}$$

and for the Al_2O_3 component

$$Mg_2SiO_4 + Al_2O_3 = MgSiO_3 + MgAl_2O_4 \quad (35)$$

forsterite liquid orthoen- statite spinel

and

$$3CaMgSi_2O_6 + Al_2O_3 = Ca_3Al_2Si_3O_{12} + 3MgSiO_3 \quad (36)$$

diopside liquid garnet orthoen- statite

and for the $NaAlSi_3O_8$ component

$$NaAlSi_3O_8 + Mg_2SiO_4 = 2MgSiO_3 + NaAlSi_2O_6 \quad (37)$$

liquid forsterite orthoen- statite jadeite

and for the TiO_2 component

$$TiO_2 + Mg_2SiO_4 + Fe_2SiO_4 = 2MgSiO_3 + Fe_2TiO_4 \quad (38)$$

liquid forsterite fayalite orthoen- static ulvo- spinel

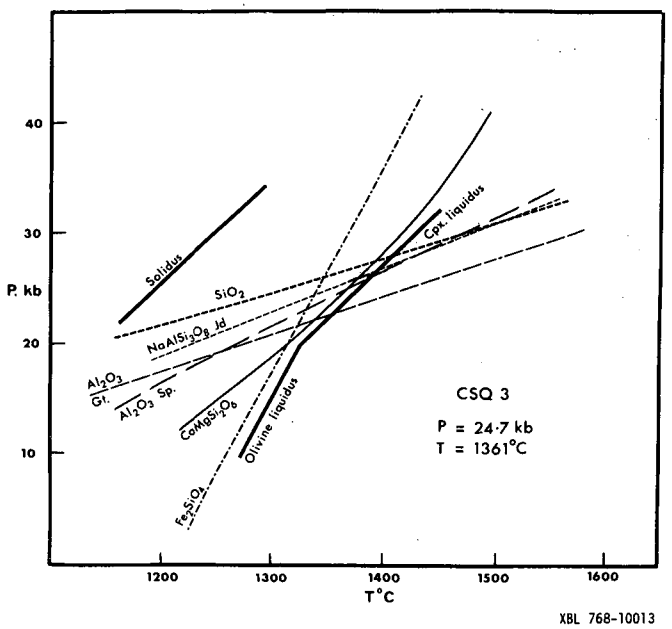

Fig. 8. Plot of calculated equilibration lines for a basanite lava CSQ-3 for various components with a stipulated solid residue. Thus SiO_2 refers to equilibration of the SiO_2 component in the lava with olivine + orthopyroxene; Al_2O_3 Gt. to the component Al_2O_3 in the lava with garnet etc. (equation 36); Al_2O_3 Sp. to the component Al_2O_3 in the lava with spinel etc. (equation 35); $NaAlSi_3O_8$ Jd to the $NaAlSi_3O_8$ in the lava with jadeite, etc. (equation 37); $CaMgSi_2O_6$ and Fe_2SiO_4 in the lava with solid $CaMgSi_2O_6$ (a = 0.4) and olivine (Fa_{15}) respectively. The solidus, olivine-liquidus and augite (cpx) -liquidus are taken from Arculus (1975) for a basanite of similar composition.

Typical results for a basanite lava are shown in Figure 8, in which it can be seen that the calculated olivine-liquid equilibration has a slope almost identical to that segment of the olivine liquidus of a similar basanitic lava (Arculus, 1975); the calculated augite-liquid equilibration also matches closely the segment of the pyroxene liquidus found by Arculus. However the composition of the olivine is Fa_{15} rather than Fa_{10} which is the typical olivine composition of lherzolite nodules; perhaps the olivine stable at depth in these basanitic lavas is more Fe-rich and the cause of this may lie in the small water content of these lavas at depth. Note that in Figure 8 the calculated P-T equilibration lines extend into the unstable regions, i.e. both above the experimental liquids and below the solidus, so that it behooves one to check that the calculated P-T equilibration conditions do lie in the stable liquid region of the lava.

The calculated equilibration values for a variety lava types are given in Table 11, and for all, the same composition of solid residue is assumed, with the exception of the olivine-tholeiites and the potassic lavas, olivine-orendite and ugandite.

Olivine-tholeiites

The two Icelandic olivine-tholeiites equilibrate with a postulated mantle residue at relatively low pressures and temperatures, close to the transition plagioclase-spinel in pyrolite (Figure 9; Green, 1970); accordingly garnet as a phase was omitted from the calculations. It is satisfying to find that these two lavas plot above the anhydrous pyrolite solidus, and in the spinel field, for O'Nions and Grönvold (1973) have shown that Icelandic olivine-tholeiites do not have an Eu anomaly. Thus plagioclase was either completely consumed in their generation, or the ambient oxygen fugacity suppressed the Eu anomaly (Weill and Drake, 1973), or plagioclase was not a phase contributing to these partial melts.

Basanites and Alkali-Basalts

The basanites and alkali-basalts all plot in an area in Figure 9 which suggests that they were in equilibrium with a solid residue at temperatures below the anhydrous pyrolite solidus. The solid residue in this case includes garnet and spinel, and although these two minerals may be antipathetic in simple silicate systems, with spinel transforming to garnet with increasing pressure, a spinel phase is found in many garnet-lherzolites, and also as an inclusion in diamond (Meyer and Boyd, 1972), which suggests that it is stable as a Cr-rich

TABLE 11

Calculated equilibration pressures and temperatures with solid residue defined in the text. The calculated activities of Fe_2TiO_4 in this residue are given for the average equilibration conditions. The errors are discussed in the text and are considered to be ± 40° and ± 5.7 kbars.

Lava-type Basanites	Pressure (kbars)	Temperature °C	$a_{Fe_2TiO_4}$
253	22.8	1314	0.0049
256	22.4	1311	0.0052
CSQ-3	24.7	1361	0.0049
CSQ-28	24.1	1356	0.0050
Alkali-basalts of Lake Rudolph, Kenya			
SIC-3	26.2	1335	0.0055
SSC-7	24.1	1412	0.0058
High-alumina basalt, Hat Creek, California			
Cal 63	24.1	1393	0.0046
Leucite-basanites of Vesuvius			
1760 AD flow 94-14	17.6	1261	-
1631 AD flow 94-18	20.8	1274	-
Olivine tholeiites, Thingmuli, Iceland			
H-128	12.6	1311	0.014
H-6	9.8	1272	0.015
Makaopuhi Lava Lake, Hawaii	6.5	1280	-
Ugandite, African Rift Valley, Uganda			
U-111	>60.0	>1350	

Data on the lavas taken from Bacon and Carmichael (1973), Brown and Carmichael (1971), Brown (1971), Smith and Carmichael (1968, 1969), Carmichael (1964, 1967a,b) Wright and Weiblen (1967), and unpublished data on the leucite-basanites of Vesuvius.

variety to very high pressures. The calculated activity of Fe_2TiO_4 in the spinel at the equilibration conditions is significantly smaller ($a_{Fe_2TiO_4}$ ~0.005) than for the tholeiites.

Green (1973b) has determined the liquidus relationships, with and without water, of a basanitic liquid, and his results are depicted in Figure 10, together with the calculated P-T values of the lavas taken from Table 11. If the small stability field of orthopyroxene is appropriate to all these lavas, then each should fall at the junction of the orthopyroxene field with garnet, olivine and augite, the stipulated solid residue. As the effect of water has not been taken account of explicitly in the calculations, either by assuming the effect of diluting the components without any specific interaction with an individual component, or by assuming a specific interaction, the lack of correspondence of the plotted points with the anhydrous pyrolite solidus could be the result of errors in the thermodynamic data.

The concentrations of trace-elements, particularly their enrichment in the light rare-earths, have suggested that basanite liquids were in equilibrium with garnet at depth (Gast, 1968, Kay and Gast, 1973); the writers, while not suggesting otherwise, are reticent to accept any melting model of source material which excludes apatite, in which the light rare-earths are strongly enriched (Carmichael, 1967a), especially as basanitic lavas show a correlation between the concentration of phosphorous and rare-earths (e.g. Arculus and Shimizu, 1974).

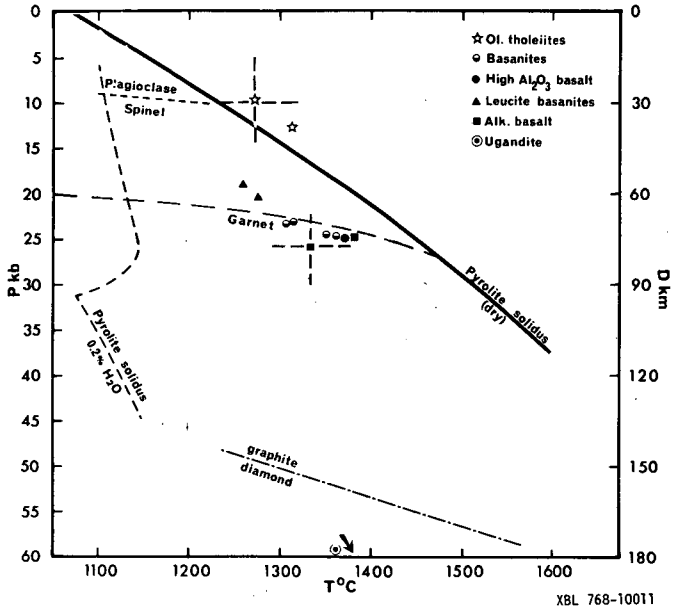

Fig. 9. Calculated equilibration pressures and temperatures (Table 11) plotted in relation to the melting temperatures of pyrolite. The dry and wet pyrolite solidus curves are taken from Green (1973), the plagioclase-spinel boundary from Green (1970) and the spinel-garnet boundary from O'Hara et al. (1971). Typical errors (±40°; ±5.7 kbars) are shown for two lava types.

The calculated equilibration conditions of this lava type with the solid residue fall in the spinel stability field of pyrolite in accord with the subdued rare-earth pattern of this lava type (Gast, 1968), which suggests that garnet was not a residual phase.

Highly Potassic Lavas

Ugandite lavas and cinder cones in the African Rift valley (Brown, 1971) are geographically associated with sporadic diamonds (Reece, 1961) which would suggest that the source region of this magma type is in the diamond stability field (Fig. 9). However it was impossible to obtain the types of intersection shown in Fig. 8 unless pyroxene with a high activity of the $CaMgSi_2O_6$ component was used. Thus the calculated equilibration conditions are very uncertain (Table 11), but fall in the diamond field. However small amounts of CO_2 dissolved in the magma would tend to raise the activity of silica, as CO_2 causes the precipitation of enstatite in the system Mg_2SiO_4 -Ca_2SiO_4 (Eggler, 1975) and would thus reduce both the calculated temperature and pressure.

It should be apparent that the calculated equilibration conditions for all the various lava types depend completely upon the choice made for the composition of the minerals in the solid residue. Perhaps a more fruitful approach would be to reiterate the calculations by changing the composition of the solid solutions until all the curves intersected at a point in P-T space. As temperature shows such a sensitive response to change in composition (cf Fig. 7), the calculated conditions may not be very different to those shown in Table 11.

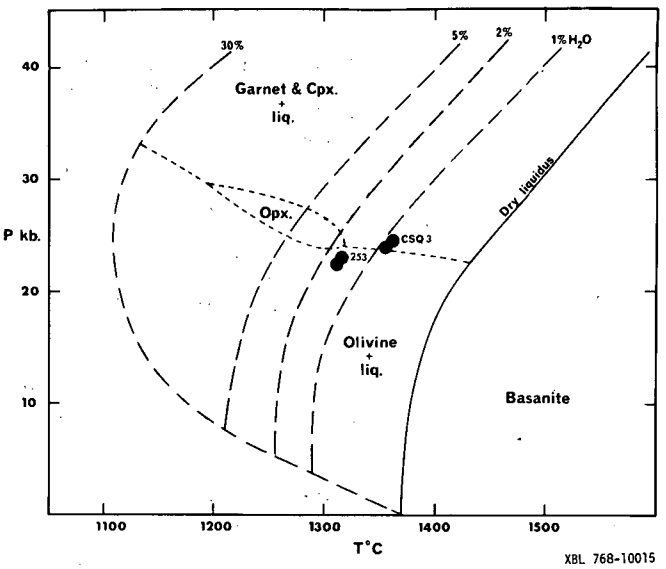

Fig. 10. Experimental liquidus temperatures and stability fields for various amounts of water (weight percent) for a basanite lava (Green, 1973). The four basanites of Table 11 are plotted, and indicate water contents of less than 2%.

Ultrabasic Nodules, Basanites and their Megacrysts

The occurrence of ultrabasic nodules, often well rounded, is a distinctive feature of basanite lavas both on the continents and on the continental side of island arcs. Very often these nodules display internal equilibration temperatures (MacGregor and Basu, 1974) which are much lower than those of the lava at any point in its ascent. Although the internal equilibration temperatures and pressures are based essentially on the extrapolation of the $CaMgSi_2O_6$ - $MgSiO_3$ solvus (Boyd, 1973; Mercier and Carter, 1975) to natural pyroxenes, there is a great range even within one nodule (Wilshire and Jackson, 1974), and the inferred conditions seem highly uncertain. This evidence, coupled with the Sr isotopic data (Stueber and Ikramuddin, 1974), suggests that many nodules are foreign to the lavas in which they are found and it seems unlikely that any of the nodules represent crystalline source material expelled with the lava. However, if ultrabasic nodules, representing an internal equilibration range of 800-1100°C and approximately 3-30 kilobars (MacGregor and Basu, op. cit.) become engulfed in the lava on its ascent to the surface, there must be a thermal response of the hot magma (1200-1350°C) to the cooler nodules. One such response could be the precipitation of crystals, namely the megacrysts that are commonly found in nodule-containing basanite lavas.

As the ultrabasic nodules can only be incorporated from the mantle, at depths roughly speaking in excess of 35 kms for the continental basanites, the equilibration of the megacryst assemblage should indicate pressures greater than this, and temperatures appropriate to the lava liquidus. One of the curious features of megacrysts (Bacon and Carmichael, 1973) is that they are almost unzoned compositionally, but there may be several

different compositional populations of the same phase. These populations often show only a small range in composition.

Binns et al. (1970) provide abundant analytical data on the composition of the megacrysts found in an Armidale (NSW) basanite. The phases present as large crystals are augite, olivine, orthopyroxene, feldspar, spinel and zircon. By using the relevant activity coefficients noted above, the following solid-solid reactions can be plotted as curves in P-T space on the assumption that the assemblage of megacrysts is in equilibrium:

$$CaMgSi_2O_6 + MgSiO_3 + MgAl_2O_4$$

solid orthoen-statite solid

$$= CaAl_2Si_2O_8 + Mg_2SiO_4 \quad (39)$$

solid solid

and

$$NaAlSi_2O_6 + 2MgSiO_3 = NaAlSi_3O_8 + Mg_2SiO_4 \quad (40)$$

solid orthoen-statite solid solid

$$ZrO_2 + 2MgSiO_3 = Mg_2SiO_4 + ZrSiO_4 \quad (41)$$

solid orthoenstatite solid solid

Note that as ZrO_2 is absent among the megacryst assemblage, the equilibration conditions have to be confined to the olivine-zircon field.

If the composition of the lava containing the megacrysts is also known (including the composition of all the mineral phases), then by using equation 33, the P-T lines of equilibration can be plotted for the lava with each type of megacryst. For the two basanites from San Quintin, Baja California (Bacon and Carmichael, 1973), the megacrysts are assumed to be common to both, and the following results are obtained:

		P(k bars)	T°C
Armidale basanite		20.0	1225
San Quintin basanites	CSQ-3	17.3	1236
	CSQ-28	16.0	1234

These results are plotted in Figure 11 and show that for any reasonable depth of mantle, the megacryst assemblage, assumed to be in equilibrium, corresponds to mantle pressures. Green and Hibberson (1970) were able to duplicate experimentally the composition of the pyroxene megacrysts found in an alkali-basalt, and with approximately 2% H_2O in the liquid, the required conditions were 1200°C and 14-16 k bars (Figure 11). However a sodium-rich feldspar was not recorded in these experiments, and has not been found experimentally at high pressures near the liquidus (Green and Ringwood, 1967; Irving, 1974). The very common

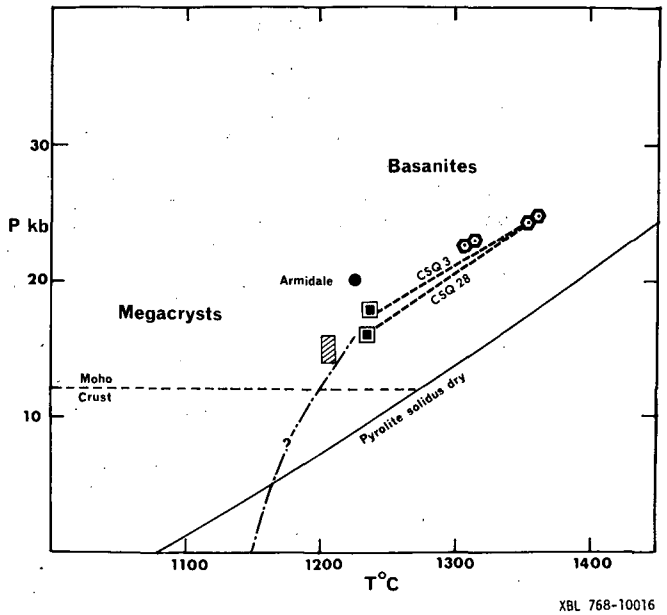

Fig. 11. The calculated equilibration conditions of the megacryst assemblage of the San Quentin basanites are plotted, and connected by dashed lines to their lavas (Table 11). The dot labelled Armidale refers to the megacrysts described by Binns et al. (1970), and the shaded area to the experimental conditions required to duplicate the composition of the pyroxene megacrysts in an alkali basalt (Green and Hibberson, 1970).

occurrence of virtually unzoned feldspar megacrysts in nodule-bearing alkali basalt is difficult to reconcile with the present hydrous experimental data, and recent strontium isotopic evidence is ambiguous, for in the Ross Island basanites of Antarctica (Stuckless and Ericksen, 1976) the megacrysts of tianiferous augite, kaersutite and anorthoclase are all in isotopic equilibrium with the host basalts, but in the basanites of south-eastern Australia, only the augite megacrysts are in equilibrium (Stuckless and Irving, 1976).

As the megacrysts from the Mexican basanites are unzoned, we may speculate that they precipitated and grew so quickly that their composition was unaffected by any change of P and T in the upward trajectory of the magma. Let it arbitrarily be taken that a change of less than 1 kilobar (≡ 3 kms) is without detectable effect on the composition of the crystals. Thus in the time taken to traverse this distance, approximately 6×10^3 seconds the feldspar crystals must nucleate and grow to a length of 2 cms or so, which necessitates a growth rate of 3.3×10^{-4} cms/sec. This is a factor of 2 greater than the maximum growth rate (120° below the liquidus) for feldspar in lunar liquids (Scherer et al., 1972), but slower than the growth rate of anorthite in $CaAl_2Si_2O_8$ liquid 25° below the liquidus temperature (Klein and Uhlmann, 1974). As the motion of rapidly ascending magma would ensure a plentiful supply of nutrients for the growing crystal, comparison with a growth rate determined for crystals growing from liquids of their own composition may be appropriate.

Water in Basaltic Source Regions

Of the estimates of the pristine water content of basaltic magma, those by Moore (1970) are the most elegant and satisfying. In round numbers, tholeiitic basalts of Kilauea type contain 0.5% by weight, whereas more alkali-rich basalts contain 0.9%. The relationship found by him between the concentration of water (H_2O^+) and P_2O_5 suggests that basanites contain approximately 1-1.4%, which is in general conformity to the position of the equilibration points shown in Figure 10.

In general terms, the experimental results on basaltic lavas show that the addition of H_2O lowers silica activity compared to the anhydrous liquids; in a Paricutin andesite orthopyroxene is stable in the absence of water, but with the addition of small amounts of water equivalent to a vapor pressure of 300 bars, olivine becomes stable (Eggler, 1972). Nicholls and Ringwood (1973) have also remarked on the effect of increasing water concentration promoting the stability of olivine in tholeiitic liquids; Mysen and Boettcher (1975) so reduced the activity of silica in an andesite liquid by the addition of water that they were able to equilibrate the andesite with a peridotitic crystalline residue. These results necessitate (at constant temperature) an increase in pressure for the equilibration of a hydrous basaltic magma, compared to an anhydrous magma, with a solid residue of orthopyroxene and olivine. The effect of pressure on all solid assemblages which could define silica activity of the source regions is to lower the silica activity (Nicholls et al., 1971), and if that of the magma, or partial melt, is reduced by addition of water, then the equilibration pressure for the same solid residue must be greater compared to an anhydrous partial melt (cf. the effect of CO_2 noted above).

One way in which the addition of water in the inverse path can be taken into account in the calculations is to assume that water acts only to dilute the other components in the magma; this is a corollary of Burnham's (1975) claim that water mixes ideally in basaltic magmas. If it is assumed that 1%, 2%, or 4% H_2O was present, then new values of X_i and ϕ_i for each lava are calculated, and the whole procedure repeated of plotting P-T lines of equilibration (Figure 8) for each concentration of H_2O. The calculated P-T equilibration conditions are unaffected by such a non-specific dilution.

Basaltic lavas with between 1-2% H_2O would only be saturated with H_2O at depths of a kilometer or less (Hamilton et al., 1964), and at all greater depths would be unsaturated. The possibility arises that during their ascent water was able to diffuse out of the magma into the surrounding mantle. This will be calculated in the next part of this paper as the time of ascent is known within limits, and the diffusion rate of water in basaltic magma may be approximated by Shaw's (1974) measurements on diffusion of H_2O in siliceous obsidian.

Water as a Thermodynamic Component

Water in the mantle resides either in hydrous phases such as phlogopitic mica or pargasitic amphibole, both perhaps containing significant amounts of fluorine (Holloway, 1973) or in some combination of fluid inclusions crystallographic vacancies and defects or as a chemisorbed hydroxylated surface layer.* To illustrate a calculation which takes explicit account of the specific thermodynamic properties of water as a component we consider a mantle assemblage containing phlogopitic mica. This is not an unreasonable choice for alkalic basalts in general and the highly potassic lavas in particular since potash must be present in the source regions. We assume that the fugacity of water is buffered by phlogopite and write the following reaction:

$$\underset{\text{phlogopite}}{KMg_3AlSi_3O_{10}(OH)} + \underset{\text{orthoenstatite}}{3MgSiO_3} \rightleftharpoons \underset{\text{forsterite}}{3Mg_2SiO_4} + \underset{\text{liquid}}{KAlSi_3O_8} + \underset{\text{steam}}{H_2O} \qquad (42)$$

Since we are interested in predicting water contents we need as auxillary information free energy data for the reaction

$$\underset{\text{(in silicate liquid)}}{H_2O} \rightleftharpoons \underset{\text{(steam)}}{H_2O} \qquad (43)$$

Spera and Hildreth (1974) have considered this problem and have calculated the temperature dependence of the Henry's law constant for reaction 43 by numerically determining limiting Henry's law

$$(\gamma^{liq}_{H_2O} \rightarrow 1 \text{ as } X^{liq}_{H_2O} \rightarrow 0)$$

slopes on $f^{v}_{H_2O}$ (fugacity of H_2O in vapor phase) vs

$(X^{liq}_{H_2O})^2$ (square of mole fraction H_2O in liquid)

curves for a series of rock-water systems in which R (Lacy, 1955), the ratio of oxygen to network forming cations, ranged from about 2 to 2.4. Burnham (1975) concluded that deviations from ideality generally were insignificant (i.e., $\gamma^{liq}_{H_2O} = 1$) in $NaAlSi_3O_8$ liquids with less than about 6 wt. % H_2O. The equilibrium constant calculated by these methods for reaction 43 becomes

---

*There are, in general, two sorts of adsorption. Physically adsorbed water is water rather loosely held on a surface layer by van der Waals type forces (bond energies of order 2-5 k cal $mole^{-1}$) and can be several tens or hundreds of water molecules thick. Chemisorbed water is held by actual chemical reation of water with the surface of the adsorbent probably to form OH^- groups, presumably in the same manner as H_2O reacts with silicate liquids at low H_2O concentration (Burnham and Davis, 1974). Chemisorbed water, by necessity is one molecular layer thick and is the dominant form of sorption at high temperatures since it is characterized by somewhat larger bond energies (12-20 k cal) than physical adsorption.

$$\ln K = \ln f^{v}_{H_2O} - \ln a^{liq}_{H_2O} = -\frac{\Delta G^\circ_{43}}{RT}$$

$$= -\frac{2854}{T} + 12.361 \qquad (44)$$

where a solute standard state has been adopted

(i.e., $\gamma^{liq}_{H_2O} \rightarrow 1$ as $X^{liq}_{H_2O} \rightarrow 0$)

and where the activity of water in the liquid with respect to a sliding reference state in P and T becomes

$$a^{liq}_{H_2O} = (X^{liq}_{H_2O})^2 \qquad (45)$$

The original polybaric and isothermal data apply strictly in the range from about 800°C to 1200°C but the simple nature of the lnK expression allows extrapolation to high temperature without eccentric behavior. Equation 44 pertains to systems under a total pressure (P_t) of 1 bar. In order to use equation 44 at mantle pressures we need partial molar volume data for H_2O in silicate melts so that we may determine the effect of P_{total} on the free energy of H_2O in the liquid

$$\left(\mu^{liq}_{H_2O}(P,T_o) - \mu^{liq}_{H_2O}(P_o,T_o) = \int_{P_o}^{P} \bar{V}^{liq}_{H_2O}\, dP\right) \qquad (46)$$

Burnham and Davis (1971, 1974) have presented P - $\bar{V}_{H_2O}$ - T data for $NaAlSi_3O_8$ liquids (R=2) and have shown that $\bar{V}^{liq}_{H_2O}$ is independent of composition. In the calculations which follow we have used their data for $P_t \leq 10$ Kb. For $P_t > 10$ kbs we have adopted a simple first order Taylor expansion equation of state for $\bar{V}^{liq}_{H_2O}$ given by

$$\bar{V}^{liq}_{H_2O} = (1 + \alpha(T-1273) - \beta(P-10000)) \qquad (47)$$

where

$$\alpha \equiv \frac{1}{\bar{V}_{H_2O}}\left(\frac{\partial \bar{V}_{H_2O}}{\partial T}\right)_P , \qquad (48)$$

the isobaric expansivity and

$$\beta \equiv \frac{-1}{\bar{V}_{H_2O}}\left(\frac{\partial \bar{V}_{H_2O}}{\partial P}\right)_T , \qquad (49)$$

the isothermal compressibility and both are calculated from Burnham's (op. cit.) $\bar{V}^{liq}_{H_2O}$ equation. Thus the equilibrium constant defining reaction 43 becomes

$$\ln K = \ln f_{H_2O} - \ln a^{liq}_{H_2O} = \frac{-2854}{T} + 12.631$$

$$+ \int_0^{10000} \frac{\bar{V}^{liq}_{H_2O}}{RT}\, dP + \int_{10000}^{P} \frac{\bar{V}^{liq}_{H_2O}}{RT}\, dP \qquad (50)$$

where the first integral is based on the Burnham and Davis (op. cit.) expression for $\bar{V}^{liq}_{H_2O}$ and the second on that given above*.

By adding reaction 42 and 43 and rearranging we can generate an expression which defines the activity of the component $KAlSi_3O_8$ relative to a liquid standard state as a function of P_t, T and $X^{liq}_{H_2O}$.

$$\ln a^{liquid}_{KAlSi_3O_8} = 3 \ln a^{pyroxene}_{MgSiO_3} - 3 \ln a^{olivine}_{Mg_2SiO_4}$$

$$+ \ln a^{mica}_{KMg_3AlSi_3O_{10}(OH)_2} - 2 \ln X^{liq}_{H_2O}$$

$$+ \frac{\Delta G^\circ_{43} - G^\circ_{42}}{RT} - \int_1^P \frac{\Delta V^\circ}{RT}\, dP$$

$$- \int_1^{10000} \frac{\bar{V}^{liq}_{H_2O}}{RT}\, dP - \int_{10000}^{P} \frac{\bar{V}^{liq}_{H_2O}}{RT}\, dP \qquad (53)$$

Since equation 53 gives the activity of $KAlSi_3O_8$ in the model mantle source assemblage, all that remains is to write an equation that expresses the activity of $KAlSi_3O_8$ in a liquid unbuffered by the presence of solids.

Calculation of X_{H_2O}

If an estimate of the activity of $KAlSi_3O_8$ in the lavas can be made (reaction 9), then a value can be calculated for X_{H_2O} at the equilibration pressure and temperature (Table 11) by using equation 53 equated to equation 32 for the $KAlSi_3O_8$ component. We have used as an example two basanite lavas which contain alkali-feldspar in the groundmass (Smith and Carmichael, 1968). However in

---

*Written out in full for $P_t \leq 10$ Kb we have

$$\ln K = -\frac{2854}{T} + 12.631 + P\left(\frac{0.10998}{T} + 4.432 \times 10^{-5} + 1.4048 \times 10^{-7} T - 2.3935 \times 10^{-11} T^2\right)$$

$$+ P^2\left(\frac{7.3365 \times 10^{-8}}{T} - 1.1696 \times 10^{-8} - 9.5 \times 10^{-13} T\right) + P^3\left(\frac{1.876 \times 10^{-10}}{T} + 4.5863 \times 10^{-13}\right) + P^4\left(-\frac{1.191 \times 10^{-14}}{T}\right) \qquad (51)$$

Written out in full, for $P_t > 10$ Kb we have

$$\ln K = -\frac{1948}{T} + 10.954 + 1.41 \times 10^{-4} P + .032\left(\frac{P}{T}\right) - 5.03 \times 10^{-7}\left(\frac{P^2}{T}\right) + 1.31 \times 10^{-3} T - 2.4 \times 10^{-7} T^2 \qquad (52)$$

TABLE 12

Calculated Water Contents in Equilibrium with Phlogopitic Mica

Sample	T_{quench} °C	$\phi_{KAlSi_3O_8}$	$a_{KMg_3AlSi_3O_{10}(OH)_2}$	P_{total} bars	T °C	f_{H_2O} bars	P_{H_2O}† bars	$X^{liq}_{H_2O}$	Wt.%H_2O*
253	980	1047	0.10	22800	1314	4807	804	.044	1.27 ± 0.50
253	980	1047	0.21	22800	1314	10095	1687	.064	1.87 ± 0.50
256	995	1130	0.10	22400	1311	4697	786	.045	1.31 ± 0.50
256	995	1130	0.21	22400	1311	9863	1469	.065	1.93 ± 0.50

*Calculated using wt. % $H_2O = 1800\ X^{liq}_{H_2O}/(gfw + X^{liq}_{H_2O}(18 - gfw))$ where gfw (253) = 64.2 and gfw (256) = 64.9.

†Calculated using estimated $\gamma^{v}_{H_2O}$ values from Spera (1974).

order to calculate X_{H_2O}, it is necessary to estimate the activity of hydroxy phlogopite (equation 53), and we have assumed that the mica has the same composition as the magnesian biotite of a Tanzanian peridotite nodule (Dawson et al., 1970) and for which we calculate by the ionic mixing - probability model described earlier

$$a^{mica}_{KMg_3AlSi_3O_{10}(OH)_2} = 0.21.$$

Flower (1971) has also analysed a phlogopitic mica from Jan Mayen in the North Atlantic and his composition gives a lower activity (0.10) since fluorine was included in his analysis. The activities of $MgSiO_3$ and Mg_2SiO_4 are taken as 0.73 and 0.81 respectively.

For the two basanites 253 and 256 we obtain the results shown in Table 12. The agreement between the calculated results and the values deduced from Figure 10 for these two basanites seems satisfactory especially considering the uncertainty in the activity of phlogopite which was used to calculate $X^{liq}_{H_2O}$. In principle, the P-T equilibration conditions should be redetermined using the newly calculated $X^{liq}_{H_2O}$ in order to calculate new ϕ_i values and the iteration continued until an internally consistent set of thermodynamic intensive variables are obtained. In practice, however, the effect of several percent H_2O will alter ϕ_i values insignificantly; the new PT equilibration values differ from the original anhydrous ones by amounts smaller than the estimated errors in determining P_{total} and T.

C. Irreversible Effects in Magma Production

Up to this point we have dealt solely with equilibrium or reversible conceptual schemes. The calculation of the intensive variables (P_E, T_E and a_i, ... a_n for n component system) are all based on the idea of chemical equilibrium, a concept of great utility but also a concept that somewhat limits the scope of inquiry. We immediately recognize the fact that from a dynamic or mechanistic point of view the eruption of lava onto the surface of the Earth is one of the last of a long chain of evolutionary instabilities characteristic of virtually all complicated chemical and mechanical systems far from equilibrium (Nicolis et al., 1975; Prigogine and Lefever, 1974). This is not to say that the results previously given in this paper are invalid; only that they must be viewed in the context of a dynamically non-linear system that is continuously evolving in time and space. As an example of the different scales and mechanical regimes that influence the final volcanic product consider the following somewhat naive and idealized sequence of instabilities that culminate in a volcanic eruption.

i. In situ production of liquid by partial fusion process; perhaps due to a thermomechanical failure; e.g., the thermal feedback problem (Shaw, 1969; Gruntfest, 1963; Shaw, 1973).

ii. Segregation of melt from isolated pockets to larger pools of liquid; if viscous failure is indeed a significant mechanism operating to produce melt the two processes would be related in that the large strain rates necessary to generate melt would also serve to coalesce the magma bubbles into large pools (Shaw, 1969; Weertman, 1971; 1972). If the region of space where magma segregation occurs is not characterized by high effective strains then a model of melt segregation such as Sleep's (1974) based on the fluid dynamics of 2 phase flow with mechanical interaction (see Faizullaev, 1969 for a detailed account of the assumptions underlying this solution) may be applicable.

iii. The relatively rapid ascent of coherent batches of magma; until this point the magma has stayed relatively close to the area where it was initially generated. Once larger bodies of melt have formed they can ascend relatively rapidly by any number of means. Two that come to mind quickly are the elastic crack propagation model (Weertman, 1971) or the viscous upwelling governed by a fluid buoyancy Rayleigh-Taylor type instability (Chandrasekkar, 1961; Ramberg, 1972; Whithead and

Luther, 1975). In the latter case the buoyant mass detaches from the growing melt layer when the Stokes law ascent rate becomes greater than the rate of growth of the viscous sphere. During this period in the life cycle of the magma a great deal of what can happen remains obscure. For one, it is during this phase that the possibility of mass transfer from rising magma to mantle or vice versa may occur. Rheologically speaking, the rising magma bodies "see" a whole spectrum of mechanical behavior patterns in the surrounding mantle as the pressure and temperature varies continuously along the path from source to surface.

iv. The storage of magma in high level chambers and final eruption; During this phase a variety of chemical and physical properties of the melt may change. Fractional crystallization and heat losses due to cooling may influence the final T-P path the magma follows. Depending on the initial volatile content and the volatile mass transfer rate the melt may eventually come to a level where a gas phase can separate. When this happens the dynamic regime changes from a solid-liquid incompressible fluid flow problem to a highly complicated 3 phase compressible fluid problem. Again the paths the magma may take in intensive variable-velocity space are many and difficult to systematize (Bennett, 1971) in terms of broad generalizations.

In the previous discussion we separated the life history of a typical eruption into a number of distinct phases. It goes without saying that we do this solely for conceptual reasons. In fact, there exists a delicate coupling between all states and it is the inherent feedback effects which dominate what we see at the surface. It is beyond the scope of this paper to report on all aspects of the various regimes briefly alluded to above. Instead we would like to look more closely at some aspects of the ascent history of magmatic bodies.

Evolution of Basanitic Magmas During Ascent

We propose now to look at some of the thermal, mechanical and chemical features that control to some extent what we as petrologists see at the surface of the Earth when studying an alkali basalt flow. We begin by gleaning information obtained directly from the sizes of ultrabasic inclusions combined with some simple (non-convective) models of fluid flow. We then turn our attention to some theoretical studies of thermal buoyancy convection in tubes in an effort to determine possible dynamothermal regimes. Finally we develop expressions for the heat, mass and momentum transfer rates following a simple boundary layer approach and then use the various flux expressions to quantitatively estimate (in conjunction with the ascent rate data) integral heat and mass exchange values. It should be noted that the results of these studies tell us something not only about the magma body but also of the medium (e.g., the mantle) the melt travels through since it is the properties of the media as well as the medium that control what we see upon eruption.

We begin by inquiring what information can be gleaned directly from observations on the size of ultramafic nodules. The behavior of spherical particles in a fluid stream can be predicted with reasonable accuracy since the problem finds many direct applications in the fluid dynamic and engineering literature (McNown and Malaika, 1950; Sutterby, 1973). The restriction to spherical particles is not a necessity as there have been empirical studies which correlate particle shape with settling velocity. The interested reader is referred to McNown and Malaika (1950) for the engineering aspects and Shaw (1965) for the geological consideration of this problem. We will treat the particles as being spherical because often xenolithic ultramafic nodules are found to be nearly so. For a non-accelerating particle in a stream, a settling velocity may be computed by balancing the buoyancy force against the viscous tractive force (frictional forces) always opposing the direction of motion. The force or drag on a sphere is generally given in terms of a drag coefficient

$$C_d = \frac{8F}{\rho_n \omega^2 D_n^2} \tag{54}$$

where F is the force acting on the sphere, and ρ_n, ω and D_n are the density, vertical velocity and nominal diameter of the equivalent spherical nodule. In the range of Reynolds numbers, Re < 0.1 where

$$Re = \frac{\rho_n D_n \omega}{\eta_L} \tag{55}$$

Stokes' law applies and

$$C_d = \frac{Re}{24} \tag{56}$$

For larger values of Re an empirical formula given by Kay (1968) gives

$$C_d = 18.0\ Re^{-0.6} \tag{57}$$

Equating buoyancy and frictional forces and rearranging gives

$$\omega = \left[\frac{4D_n(\rho_n - \rho_L)g}{3C_d\rho_L}\right]^{1/2} \tag{58}$$

where ρ_L is the fluid (magma) density and g the acceleration due to gravity (981 cm sec^{-2}). In the Stokes' law range (58) reduces to the familiar equation

$$\omega = \frac{D_n^2(\rho_n - \rho_L)g}{18\,\eta_L} \tag{59}$$

To compute the actual settling velocity in the dynamic regime where

$$Re > 0.1 \tag{60}$$

recourse may be made to an iterative solution to equations (54) and (58) to obtain an internally consistent set of parameters. As an example consider the settling velocity of an olivine-orthopyroxene nodule from Hualalai Volcano, Hawaii with a density of 3.45 g cm^{-3} and a diameter of 30

cm. Given a density and viscosity of Hualalai alkali basalt (MacDonald, 1949, p. 78, no. 1) of 2.80 g cm^{-3} and 350 poise* respectively, we calculate

$$Re = 14.9$$

$$C_d = 3.55$$

$$\omega = 50.6 \text{ cm sec}^{-1} \quad (1.8 \text{ kms hr}^{-1})$$

Using the simple Stokes' law formula one calculates

$$\omega = 91.1 \text{ cm sec}^{-1}. \quad (3.2 \text{ kms hr}^{-1})$$

Because the low Re number approximation underestimates the total drag, velocities calculated with equation (59) are in error by a significant amount. The settling velocity calculated above illustrates the fact that we are dealing with characteristic velocities of tens of cm s^{-1}, orders of magnitude greater than the characteristic velocities at which plates move about on the surface of the Earth. In fact, the settling velocities calculated in this manner are minimum magma ascent rates, since if magma was moving upwards at just this rate, a 30 cm nodule would remain at a fixed depth.

Some information regarding the geometry of an ascending magmatic bodies can be obtained from simple volumetric considerations. Lamb (1945) considered the problem of the drag on a spherical drop of fluid of radius R and viscosity η_L moving under a gravity induced buoyancy force in a fluid of viscosity η_m. For the drag we have

$$F = \frac{2\pi\omega\eta_m R(2\eta_m + 3\eta_L)}{(\eta_m + \eta_L)} \tag{61}$$

Note that

$$\lim_{\eta_L \to \infty} F = 6\pi\omega\eta_m R \quad \text{(hard sphere in viscous medium)} \tag{62}$$

and that

$$\lim_{\eta_L \to 0} F = 4\pi\omega\eta_m R \quad \text{(gas bubble in viscous medium)} \tag{63}$$

For a batch of magma ($\eta_L \simeq 10^3$ poise) rising through the mantle ($\eta_m \sim 10^{21}$) it is clear that equation (62) is applicable. Equating the buoyancy force on the magmatic sphere to the drag force we have after rearrangement for the radius of the sphere

$$\left[\frac{3\omega\eta_m}{g(\rho_m - \rho_L)}\right]^{1/2} = R \tag{64}$$

taking $\omega = 50.0$ cm sec^{-1}, $\eta_m = 10^{21}$ poise and $\Delta\rho = .60$ gm cm^{-3} we have

$$R = 1.58 \times 10^{10} \text{ cm}, \tag{65}$$

clearly an outrageously large number. This is because of the high value of the viscosity of the mantle used in the calculation and because we have neglected convection within the rising body. It may be argued, however, that there is a significant wall effect; that is the hot magma will heat a boundary layer envelope around the magma tube perhaps to temperatures high enough to begin partial fusion of the surrounding spinel or garnet peridotite thereby lowering the effective viscosity of the mantle (η_m). Let us explore this argument further by calculating from the volume of a typical nodule and magacryst bearing basanite flow the value of η_m necessary to allow the magma sphere to ascend at a typical nodule settling rate. Since viscosity is a strong function of melt fraction at temperatures between the peridotite solidus and liquidus it is informative to convert the viscosity decrement to a temperature interval and examine the mineralogical constitution of any residue of the "shell melting" episode. As an example of a nodule bearing flow take one from Black Rock Summit, Nye County, Nevada with an estimated volume of about 0.03 $Km.^3$ Converting this volume to an equivalent sphere we have

$$R = \left(\frac{3V}{4\pi}\right)^{1/3} = 1.93 \times 10^4 \text{cm (i.e., } \sim 200 \text{ m)} \tag{66}$$

With $\omega = 15$ cm sec^{-1}*, $\Delta\rho = .65$ gm cm^{-3} and $g = 981$ cm sec^{-2} we have from equation (64)

$$\eta_m = \frac{R^2 g\Delta\rho}{3\omega} = 5.3 \times 10^9 \text{ poise.} \tag{67}$$

In several papers H. R. Shaw (1969, 1973) has developed from experimental measurements and theoretical considerations a simple exponential type relation for the effective Newtonian viscosity in basaltic crystal-liquid systems at temperatures between the solidus and liquidus where the volume fraction of liquid (θ) varies continuously between 0.0 and 1.0. Although the viscosity of a solid or liquid falls with increasing temperature, the decrease is orders of magnitude greater in the melting range where the effect of decreasing concentration of suspended crystals is large. In the melting range Shaw (1969) has proposed the equation

$$\eta = \eta_s e^{-a(T-T_s)} \tag{68}$$

where η_s is the viscosity at the solidus temperature, T_s. This can be converted to an equivalent melt fraction by assuming a linear dependence of volume melt fraction θ with temperature. In this approximation we have

$$a(T-T_s) = b\theta \tag{69}$$

where both a and b are calibrated by reference to experimental data. The melting interval (ΔT_f^p) for a spinel bearing peridotite from St. Paul's Rocks is nearly independent of pressure and is about 510°C (Millhollen et al., 1974). From (69) we calculate

*Densities are calculated from the partial molar volume data of Bottinga and Weill (1970), and viscosities by Shaw's (1972) algorithm.

*This corresponds to the settling rate of a 9 cm nodule.

TABLE 13

Viscosity - Temperature - Melt Fraction Data

for Thin Shell Melting Episode

$\eta(\theta=1)$ poise	$\eta(\theta=0)$ poise	a deg^{-1}	b	θ volume melt fraction	T-Ts for peridotite °C	Phases Present (Millhollen et al., 1974) 10Kb	20Kb	30Kb
500	10^{18}	0.0691	55.23	0.54	275	spinel opx ol	opx ol	cpx opx ol
500	10^{21}	0.0826	42.14	0.62	314	ol	ol opx	ol opx
10^3	10^{18}	0.0677	34.54	0.55	281	opx ol	opx ol	opx ol
10^2	10^{18}	0.0722	36.84	0.52	364	spinel opx ol	opx ol	opx ol

The volume melt fraction (θ) and temperature decrements for the peridotitic wall material were calculated assuming an effective mantle viscosity (ηm) computed from equation (68) in the text, and ignoring heat of solution effects. To convert to a mass basis (i.e., mass melt fraction, W_L) one may use the formula

$$W_L = \frac{\rho_L \theta}{\rho_s + \theta(\rho_L - \rho_s)}$$

where ρ_L is the density of the liquid, ρ_s the density of the solid, θ the volume fraction of melt and W_L the mass fraction of melt. For small θ we have

$$W_L \simeq (\frac{\rho_L}{\rho_s})\theta$$

The shell partial melting episode may play a role in the production of vertical zones of considerable extent of depleted ultramafic rocks in the mantle. This may have some bearing on the observation by many petrologists that the inferred (by pyroxene geothermometry) temperatures of many xenoliths are considerably lower than the estimated temperatures prevailing at the time of partial fusion (i.e., the equilibration temperature, T_E).

$$\frac{a}{b} = \frac{\Delta\theta_P}{\Delta T_f} = 1.961 \times 10^{-3}\ deg^{-1}. \qquad (70)$$

Now, if we fix η such that $\eta = 5 \times 10^2$ poise for $\theta = 1$ (i.e., all liquid) and $\eta = 10^{18}$ poise for $\theta = 0$* we have

$$b = \ell n\ (10^{18}/5 \times 10^2) = 35.23 \qquad (71)$$

and

$$a = (\frac{\Delta\theta}{\Delta T_f})\ b = 0.0691 \qquad (72)$$

We determine the melt fraction necessary in the shell boundary layer to allow the viscous sphere to ascend at the required rate as

$$\theta = \frac{1}{b}\ \ell n \left(\frac{10^{18}}{5.3 \times 10^9}\right) = 0.54 \qquad (73)$$

Transforming this melt fraction into an equivalent temperature increment above the solidus we have

$$T - T_s = \frac{b\theta}{a} = 275°C \qquad (74)$$

From Figure 1 in Millhollen's paper (1974) one notes that at 275° above the peridotite solidus at 30 kbars garnet is no longer stable; calcic pyroxene, orthopyroxene and olivine are the phases remaining in the residue after the partial melting episode. Table 13 summarizes these results for a range of thermal and transport coefficients.

We can also perform a simple macroscopic energy balance and obtain information with regard to the ratio of original magma volume to the partially fused conduit wall material and an estimate of the temperature loss of the ascending magma due to the latent heat effects incurred during partial

*This is an approximation of the effective Newtonian viscosity of crystalline mantle material close to its solidus Temperature (T_s).

fusion of peridotitic wall material. The energy necessary to partially fuse an annular ring δr cm thick of radius r and length ℓ is approximately given by

$$2\pi\hat{\rho}\ (C_{P,m} + \frac{\Delta H^P_{fusion}}{\Delta T^P_f})\ r\ \delta r\ \ell\ (T-T_s) \qquad (75)$$

where we have assumed the thickness of the annular ring δr is much smaller than the radius of the magma body, r. In (75) $C_{P,m}$ is the isobaric heat capacity for the mantle, $\hat{\rho}$ is the average density of the crystal-liquid system, $T-T_s$ is the temperature increase necessary to decrease η_m to a value commensurate with the nodule (and magma) ascent velocity calculated earlier. The thermal energy lost from the original batch of fluid is given by

$$\frac{4}{3}\ \pi\hat{\rho}(C_{P,L} + \frac{\Delta H^L_f}{\Delta T^L_f})\ r^3(T_E - T) \qquad (76)$$

where ΔH^L_f is the latent heat of crystallization of the melt, ΔT^L_f is the melting interval for the magma and T_E is the equilibration temperature with the source. Equating (75) and (76) one may calculate the temperature drop experienced by the magma. The two effective heat capacity terms do not cancel because the melting interval for peridotite (ΔT^P_m) is considerably larger than for an alkali basalt (ΔT^L_m). Equating (75) and (76) and rearranging one has

$$T_E - T = \frac{3}{2}\ (C_{P,m} + \frac{\Delta H^P_f}{\Delta T^P_m})\ \frac{\delta r\ \ell}{r^2}\ (T - T_s) \qquad (77)$$

Before estimating temperature losses of the rising magma we calculate the thickness of the partially molten zone that develops in the mantle adjacent to the rising diapir. In general, the thickness of a conduction controlled boundary layer propagating into the surrounding mantle is given by an expression of the form (Meyers, 1971)

$$\delta r = \sqrt{\pi\kappa t} \qquad (78)$$

where κ is the thermal diffusivity (taken as 10^{-2} $cm^2\ s^{-1}$) and t the time in seconds. Now, if a sphere or radius r moves upwards at a velocity ω, the time any portion of the mantle will be adjacent a hot wall is roughly given by

$$t = \frac{2r}{\omega} \qquad (79)$$

and so (78) becomes

$$\delta r = (\frac{2\pi\kappa r}{\omega})^{1/2} \qquad (80)$$

Replacing δr in (77) by (80) we have finally

$$(T_E-T) = \frac{3}{2}\sqrt{2\pi}\ (C_{P,m} + \frac{\Delta H^P_{fusion}/\Delta T^P_f}{\Delta H^L_{fusion}/\Delta T_f})\ (\frac{\kappa}{\omega})^{1/2}\ \frac{\ell}{r^{3/2}}\ (T-T_s) \qquad (81)$$

With velocities on the order of several cm s^{-1} and r several hundreds of meters, δr the boundary layer thickness is of the order of several centimeters. Table 14 summarizes some of the specific numerical values implied by equations (77) and (80). It is important to note that equation (76) implicitly assumes magma temperatures are greater than the solidus of the surrounding peridotitic material. This condition will be met as long as the 1 bar solidus mantle temperature is less than or equal to about 1200°C. The pyrolite solidus of Green and Ringwood (1967) gives a 1 bar intercept of about 1175°C. However, some garnet lherzolites would project to a 1 bar solidus temperature of 1220°C (Kushiro, et al., 1972). For those bulk compositions and/or initial H_2O contents where $T_s^{1bar} > 1200°C$, the rising magma could not supply enough energy to partially fuse its peridotitic envelope thereby lowering η_m. The point we wish to make is that at early times during any given melting episode significant energy losses must be sustained by the diapir perhaps causing it to freeze at depth. Equation (77) also does not allow for any superheat in the magma. If viscous heating is important there will be no crystallization of any near liquidus phases (megacrysts) since latent heat will not contribute to the energy balance. In that case, the values for ζ, the volume fraction of melt crystallized, listed in columns 5 and 6 would be maximum values. The results summarized in Table 14 show, as one might expect, that increasing the effective volume of a magma body serves to decrease energy losses. Also note that upon increasing ω, the ascent rate, the magma body sustained a smaller temperature drop. It seems likely to the authors that rather than one pulse of magma moving up and heating its boundaries sufficiently to allow quick ascent, a whole series of such thermal pulses are responsible for the eventual "softening" of the medium surrounding the diapirs which follow in time. These considerations highlight the fact that evolving magmatic systems must be viewed within the context of the geologic history of a region. Geochronological and eruptive volume data are the basic information needed to provide the crucial link between the chemistry of the lava and the dynamics of ascent.

A slightly different argument also supports the contention that effective mantle viscosities must be orders of magnitude smaller than "nominal" isostatically derived values (if the motion is buoyancy induced). If a xenolith is to be erupted on the surface we reason that the time necessary for the nodule to settle the distance 2r, where r is the equivalent radius of the magma bubble, is greater than the time the bubble of magma rises through the superincumbent mantle and crust. Stated mathematically then the condition becomes

$$\frac{2r}{\omega} \geq \frac{Z}{U} \qquad (82)$$

where ω is the settling velocity of the xenolith (equations (54) and (56) or (57) depending on Re), Z the average depth of the magma body below the surface when the xenolith gets trapped and U the ascent rate of the less viscous magma bubble in the more viscous surrounding mantle

($U = \frac{g\Delta\rho r^2}{3\eta_m}$, see equation (62)).

TABLE 14

Summary of Energy Balance Results Calculated

by Equations 77 and 80

$T - Ts$ for peridotite	r	δr	$T_E - T$ for magma	$\zeta = 1 - \theta$	
C°	m	cm	C°	volume fraction of melt crystallized	
100	75	4.0	41 (58)	0.164	(0.232)
	100	4.6	27 (38)	0.108	(0.152)
	150	5.6	15 (21)	0.06	(0.084)
	200	6.5	10 (14)	0.04	(0.056)
	300	7.9	5 (7)	0.02	(0.028)
200	75	4.0	83 (117)	.332	(.468)
	100	4.6	54 (76)	.216	(.304)
	150	5.6	31 (44)	.124	(.176)
	200	6.5	21 (30)	.084	(.12)
	300	7.9	9 (13)	.036	(.052)
250	100	4.6	68 (96)	.272	(.384)
	200	6.5	26 (37)	.104	(.148)
	300	7.9	11 (16)	.044	(.064)
275	100	4.6	74 (105)	.296	(.420)
	200	6.5	29 (41)	.116	(.164)
	300	7.9	13 (18)	.052	(.072)
300	75	4.0	123 (174)	.492	(.696)
	100	4.6	81 (115)	.324	(.46)
	150	5.6	45 (64)	.180	(.256)
	200	6.5	32 (45)	.128	(.18)
	300	7.9	17 (24)	.068	(.096)

If effective mantle viscosities (η_m) are lowered by the partial fusion mechanism discussed, the energy required for fusion would be supplied by the latent heat effect and heat capacity of the diapir. Thicknesses of the partially molten zone (δr) and temperature decrements sustained by the magma are calculated from equations 80 and 77 respectively as a function of the temperature increase in the peridotitic rind (T-Ts) and the radius of the equivalent magma sphere. $T_E - T$ values have been converted to volume fraction crystallized ($\zeta = 1 - \theta$) where $\theta = (T_E - T)/\Delta T_f^L$ with ΔT_f^L set equal to 250°C. Assumed constant throughout are $C_{p,L} = 0.25$ cal $gm^{-1} deg^{-1}$, $\Delta H_f^p = \Delta H_f^L =$ 140 cal gm^{-1} (the heat of fusion of diopside at 1 bar and 1391°C), $\Delta T_m^p = 510$°C, $\ell = 60$ km, $\kappa = 10^{-2} cm^2 s^{-1}$, $\omega = 30$ cms^{-1}. Values in parenthesis in columns 4 and 6 are with $\omega = 15$ cms^{-1} (all other parameters identical).

TABLE 15

ηm Values Calculated Assuming the Balance

Represented by Equation 83

Z depth (km)	ηm Effective Mantle viscosity (poise)	
30	1.51×10^8	(4.47×10^7)
40	1.13×10^8	(3.34×10^7)
50	9.07×10^7	(2.69×10^7)
60	7.56×10^7	(2.24×10^7)
70	6.48×10^7	(1.92×10^7)
80	5.67×10^7	(1.68×10^7)
90	5.04×10^7	(1.49×10^7)
100	4.54×10^7	(1.34×10^7)

For the physical parameters reported in the text $Re_n = 1.31$, $C_d = 15.34$ and $\omega = 13.5$ cm s^{-1}, $D_n = 10$ cm, $\Delta\rho$ is taken as 0.6 gm cm^{-3} and $\rho_L = 2.8$ gm cm^{-3}. The first value in the table is for r = 300 m and the value in parenthesis is for r = 200 m. Z is the depth at which the nodule gets trapped by the rising magma body. Note that the values of the viscosity calculated above are in reasonable agreement with those calculated earlier in the thermal budgetary calculation.

Equation (82) finally reduces to

$$\eta_m \leq \frac{r^3}{3Z}\left[\frac{3g(\rho_n - \rho_L)C_d\rho_L}{D_n}\right]^{1/2} \qquad (83)$$

As an example, we tabulate in Table 15 maximum values of the effective viscosity of the mantle (η_m) through which the magma body rises for a 10 cm diameter nodule. The diameter of the magma body is taken to be 600 or 400 meters.

We close this section of the paper with an illustrative ascent history model. Ignoring for the moment energy losses by convection (we consider convective regimes in the next section) and viscous heating effects we note that for a body rising as fast as is inferred by the high settling velocities (of order 10 cm s^{-1}) total heat losses by conduction are small and of order (Carlslaw and Jaeger, 1959)

$$Q = 4\pi r^2 \left(\frac{Z}{\omega}\right)^{1/2} \frac{k}{\sqrt{\pi\kappa}} \Delta T_f^L \qquad (84)$$

where k is the thermal conductivity (0.007 cal dcg^{-1} s^{-1} cm^{-1}) and ΔT_f^L maximum difference in temperature across the body ($\sim$200°C). Temperature drops sustained by the body as a whole are of order

$$\frac{3Q}{4\rho_L \pi r^3 C_{P,L}} = (T_e - T)_{conduction}$$

For the 200 m radius body we have used in our reference calculations one calculates, for an ascent rate of 10 cm s^{-1} and an initial depth (Z) of 75 km,

$$(T_e - T)_{conduction} \simeq 2°C$$

One concludes from this that the significant energy sink is the latent heat involved in the partial fusion of the external boundary layer of peridotitic stuff. A 200 m radius sphere of magma moving upwards at a rate of several cm s^{-1} (as indicated by the nodule settling rate) from a depth of say 70 km, will partially fuse mantle material in a zone roughly 5 to 10 cm thick to the extent of about 20% by volume producing ol-opx or ol-opx-cpx residue. The body will cool by about 30°. The effective viscosity of the sheath of mantle the body rises through is of the order 10^8 poise. Heat losses incurred by molecular conduction will be small (e.g., not more than several degrees). The ratio of the mass added by partial fusion to the initial mass of the sphere is of order

$$\frac{3\delta r \ell \theta}{2r^2} \simeq 0.06 \qquad (85)$$

or about 6% by mass. The composition of the liquid phase that results from this partial fusion episode is that of a mildly alkaline to tholeiitic basalt (Carmichael et al., 1974).

On the Convective State of Rising Diapirs

In the discussion so far we have neglected internal convective regimes in the ascending magma body. Since it is our ultimate aim to evaluate the processes which govern the behavior of evolving magmatic systems, we now seek to develop quantitative expressions expressing local heat, mass and momentum transfer rates. In the calculations which follow the convective velocities determined are those arising in response to the temperature difference between the cool walls and the hot interior of the magma body. We recognize, however, that superimposed upon the thermal convective flow field will be a forced axisymmetric toroidal circulation pattern induced by the bulk translation of the liquid sphere at rate ω through the mantle*. Because the length scales of the two processes are very different and because of the inherent computational difficulties which arise in feedback problems we have ignored the possibility of coupling.

As the forced flow velocities are in the same direction (near the walls) as the free convective rates, one may simply add the ascent rate of the magma body (ω) to the boundary layer velocities (u) when calculating the heat and mass transfer values. This should take account (at least to a first order) of the internal flow.

* The interested reader is referred to Batchelor (1967, p. 237) or Lamb (1945, p. 600) for the equation of the stream function (ψ) for the internal toroidal flow discussed here. The tangential and radial components of the velocity may be easily computed from ψ.

The two dimensionless variables which characterize the flow regime in naturally convecting systems are the Prandtl number

$$\text{, } Pr = \nu/\kappa \tag{86}$$

and the Grashof number

$$Gr = \frac{\alpha g \Delta T r^3}{\nu^2} \tag{87}$$

where ν is the kinematic viscosity, κ the thermal diffusivity, α the isobaric expansivity and ΔT and r a characteristic temperature difference and length respectively. The product PrGr is yet another dimensionless number called the Rayleigh number,

$$Ra = PrGr. \tag{88}$$

The Pr number measures the relative rates at which momentum and energy are transferred by molecular diffusion through a given fluid. The Rayleigh number may be thought of as the ratio of buoyancy forces operating in a system (inducing flow) to the viscous forces acting to retard flow. Below a certain critical Ra number (about 10^3) viscous forces are effective in damping out any bulk flow and therefore heat is transported by molecular conduction and/or radiation. It is to a large extent, the balances amongst these various dimensionless numbers which (together with appropriate boundary conditions) determine the velocity and temperature profiles (and hence the various fluxes). The reader is referred to Shaw (1974, p. 157) for additional comments and insight into the concepts underlying the calculations which follow.

Geometrical and Scale Considerations

In what follows, we draw heavily upon the work of M. J. Lighthill (1953) who performed a rather thorough analysis of free convection in cylindrical tubes. Other workers who have contributed to this subject include Hallman (1955), Ostrach et al. (1956), Morton (1960) and Scheele et al. (1962). From the discussion in Lighthill (op. cit.) and especially from his Figures 7 and 10, it becomes apparent that for convection in a cylindrical tube of length ℓ and radius r it is the product $(r/\ell)Ra$ where

$$Ra = \frac{\alpha g \Delta T r^3}{\kappa \nu} \tag{89}$$

that characterizes the kind of flow to be expected. For example, at constant values of r and Ra as r/ℓ goes from 1.0 to 1/100 flow regimes would change from the thin boundary layer* type (BL not filling tube) to a fully developed flow with the boundary layer completely filling the tube and finally to a flow geometry where a stagnant portion of fluid would lie above or below (depending on the geometry) the fully developed laminar boundary layer flow (see figure 12 in Shaw (1965); Figures 2, 3, and 6 in Lighthill (1953)). Unfortunately it is difficult for us to obtain accurate r/ℓ values for the "tear-drop" streamlined diapirs of magma rising through the mantle. Using data from diapiric studies (Ramberg, 1968) it would seem that r/ℓ would perhaps not be much smaller than 1/20. In the calculations performed below it turns out that the dependence of the transport of fluxes on r/ℓ is negligible. At high enough values of Ra, the heat, mass and momentum transfer rates all asymptotically approach the values of the limiting case--that of free convection from a vertical plate. $T_\infty - T_w$ is the driving force behind the convective system (T_∞ represents the temperature of the magma unaffected by the presence of the wall and T_w the temperature at the boundary). We realize of course that in fact ΔT is a function of time. For instance early in the ascent history we might expect temperature differences to be smaller and for ΔT to progressively grow larger with time as the magma rises into cooler and cooler surroundings. We have chosen $T_\infty - T_w$ values to maximize the various flux quantities. The important aspect to note however is that in the Ra number the temperature difference appears to only the first power whereas length appears to the third power. The importance of estimating flow volumes is made clear by this dependence.

Free Laminar Boundary Layer Convection

Because Ra is generally so large, even for the relatively small eruptive volumes represented by alkalic basalts, the flow regime will be of the thin boundary layer character. The limiting case of laminar boundary layer flow regimes is free convection from a flat plate. This problem has been solved by Squire (quoted in Goldstein, 1938) for arbitrary Pr with the results quoted below. In forced convection problems the thermal and momentum boundary layers (δ_T and δ_M) are not of equal thickness. In fact, for flow over a flat plate

$$\delta_M = Pr^{\frac{1}{3}}\delta_T$$

(Bird et al., 1960, p. 369). In free convection problems, since it is the temperature difference which creates the buoyancy force the fluid will tend to descend only in the region where there is a temperature deficiency so δ_T has been set equal to δ_M (see Goldstein, 1938, p. 641). For combined flow problems we would expect the ratio

$$\frac{\delta_T}{\delta_M}$$

to lie somehwere between 1 and $Pr^{-\frac{1}{3}}$.

Now, the boundary layer thickness δ is given by

$$\frac{\delta}{r} = 3.93\ Ra^{-\frac{1}{4}} \tag{90}$$

* A boundary layer regime is one where temperature, velocity and concentration profiles are flat except in the neighborhood of a surface or boundary. For the boundary layer approximations to the conservation equations to be valid it must be true that $\delta << h$ where δ is the thickness of the boundary layer and h a characteristic length of the body.

with the scale velocity being given by

$$u_r = 5.17\nu \, Pr^{-\frac{1}{2}} \left[\frac{\vec{g}\alpha(T_\infty - T_w)}{\nu^2}\right]^{\frac{1}{2}} r^{\frac{1}{2}} \qquad (91)$$

The expressions for the vertical (parallel to the gravity vector) velocity and temperature are (y is measured orthogonal to g and positive into magma chamber):

$$u = u_r \frac{y}{\delta}(1 - \frac{y}{\delta})^2 \qquad (92)$$

$$\frac{T - T_\infty}{T_w - T_\infty} = (1 - \frac{y}{\delta})^2 \qquad (93)$$

From (93) we calculate for the heat flux

$$\vec{q} = -k \frac{\partial T}{\partial y} = \frac{2k(T_w - T_\infty)}{\delta}(1 - \frac{y}{\delta}) \qquad (94)$$

so that at the wall (y = 0)

$$\vec{q}_w = -k \left.\frac{\partial T}{\partial y}\right|_{y=0} = \frac{2k(T_w - T_\infty)}{\delta} \qquad (95)$$

Finally, the Nusselt number defined as

$$Nu \equiv \frac{Qr}{kS(T_\infty - T_w)} = \frac{\vec{q}_w r}{k\Delta T} \qquad (96)$$

where Q is the quantity of heat transferred per unit time from a body of surface S, characteristic length r and thermal conductivity k, depends on Ra in the following fashion

$$Nu = 0.508 \, Ra^{1/4} \qquad (97)$$

Gathered in Table 16 are the summarized results calculated by means of equations (90) through (97). It should be noted that the Squire solution does not permit a vertical velocity outside the boundary layer and furthermore assumes

$$\delta_T = \delta_M. \qquad (98)$$

Lighthill (op. cit.) has in his classic paper lifted the former constraint. As the results of his calculations are not much different than those given here we will not treat his results in any detail.

Free Turbulent Boundary Layer Convection

Examination of Figure 10 in Lighthill (op. cit.) or Figure 10 in Shaw (1965) indicates that for most choices of the governing parameters (e.g., α, g, ΔT, r, ν, κ and ℓ) rising alkali basalt systems will lie in a turbulent convective dynamic regime. That is, for the most part, calculated values of Ra are greater than 10^{10}. Summarized below are the equations governing the temperature and velocity fields in turbulent regimes. These were derived by Eckert and Jackson (1950) from integral forms of the conservation equations and are quoted from Rohsenow and Choi (1962). The derivation assumes $\delta_T = \delta_M$. Calculations were also performed using the results from a mixing-length type formulation by Kraichnan (1962), which does not suppose $\delta_M = \delta_T$. Calculated results from the two methods appeared broadly compatible. For the sake of brevity, Table 16 lists the results of the integral theory only. This should facilitate comparison of results with the laminar theory since the assumptions about δ_T and δ_M are the same. The equations used to calculate the results in parentheses in Table 16 are as follows (these are analogous to equations 90 through 97 in the laminar case):

$$\frac{\delta}{r} = 0.527 \, Ra^{-1/10} \, Pr^{-11/30} \qquad (99)$$

$$u_r = \frac{1.69\,\nu}{r} Ra^{1/2} \, Pr^{-5/6} \qquad (100)$$

$$u = u_r (\frac{y}{\delta})^{1/7} (1 - \frac{y}{\delta})^4 \qquad (101)$$

$$\frac{T - T_\infty}{T_w - T_\infty} = (1 - (\frac{y}{\delta})^{1/7}) \qquad (102)$$

All entries are calculated using a length scale defined by a right cylinder where $r/\ell = 1$ so that $r = (V/\pi)^{1/3}$ where V is the volume of the magma chamber. The y coordinate axis is taken as positive into the magma chamber. The following parameters are taken as constant throughout:

$\kappa = 10^{-2} cm^2 s^{-1}$

$\alpha = 5 \times 10^{-5}$ deg K^{-1}

$g = 981 \, cm^2 s^{-1}$

$k = 0.007$ cal $cm^{-1} deg^{-1} s^{-1}$

$Z = 75$ Km

$\rho_L = 2.70$ gm cm^{-3}

$C_p = 0.30$ cal $gm^{-1} deg \, K^{-1}$

$\omega = 10$ cm s^{-1}

$T_\infty - T_w = 200°$ K

For laminar flow note that u attains its maximum value at $y = \delta/3$ where $u_{max} = (4/27)u_r$. In turbulence u_{max} occurs at $y = \delta/29$ where $u_{max} = 0.54\, u_r$ $(T_E - T)$ is calculated from the definition of Nu and the volume of the magma body by means of the expression $(T_E - T)$

$$(T_E - T) = \frac{4\pi krz(T_\infty - T_w)Nu}{\rho_L C_{P,L} \omega V} \qquad (T16)$$

where Z is the depth at which ascent begins and ω the rate of ascent. $(T_E - T)$ does not include latent heat effects such as the partial fusion of wall rock material. For that contribution to the temperature drop see values of $(T_E - T)$ in Table 14. Values in parenthesis are calculated by the equations for turbulent flow (equations 99 through 105). The inset to the table gives the value of δ_M/δ_T calculated from Kraichnan (1962) for turbulent flow and from Bird et al. (1961) for laminar flow over a horizontal plate.

TABLE 16

Volume	Kinematic viscosity	Prandtl number	Rayleigh number	Nusselt* number	Heat Flux at boundary* $\vec{q}=-k\left.\frac{\partial T}{\partial y}\right\|_{y=0}$	Boundary layer thickness* δ	Maximum boundary layer* velocity $u_m=\frac{4}{27}u_r$ at $y=\frac{\delta}{3}$ laminar; $u_m=.54u_r$ at $y=\frac{\delta}{29}$ (turbulent)	(Te-T)*
km^3	cm^2s^{-1}	(Pr)	(Ra)	(Nu)	(cal $cm^{-2}s^{-1}$)	(cm)	($cm\ s^{-1}$)	(°C)
0.03	$2x10^2$	$2x10^4$	$4.7x10^{13}$	1330 (4691)	$8.75x10^{-2}$ ($31.0x10^{-2}$)	32 (13)	3.0 (15)	15 (53)
0.03	50	$5x10^3$	$1.9x10^{14}$	1881 (7474)	$12.5x10^{-2}$ ($49.0x10^{-2}$)	22 (18)	5.0 (25)	21 (86)
0.185§	$2x10^2$	$2x10^4$	$2.9x10^{14}$	2096 (8605)	$7.56x10^{-2}$ ($31.0x10^{-2}$)	37 (19)	3.0 (39)	7 (29)
0.185	50	$5x10^3$	$1.2x10^{15}$	2972 (13815)	$10.7x10^{-2}$ ($50.0x10^{-2}$)	26 (28)	7.0 (62)	10 (47)
0.03	$5.0x10^2$	5.10^4	$1.9x10^{13}$	1061 (3469)	$7.0x10^{-2}$ ($23.0x10^{-2}$)	40 (10)	2.6 (11)	12 (39)

§ This is an estimate of the eruption of the remarkable Kanpulehu flow of the 1801 eruption of Hualalai Volcano, Hawaii

* Values for turbulent flow regime in parenthesis

Pr	$\frac{\delta_m}{\delta_T}=3.2\ Pr^{1/2}$ (turbulent)†	$\frac{\delta_m}{\delta_T}=Pr^{1/3}$ (laminar)†
$5x10^3$	226	17
$1x10^4$	320	22
$2.5x10^4$	506	29
$3.5x10^4$	599	33
$5x10^4$	716	37

† $\frac{\delta_m}{\delta_T}$ for turbulent flow calculated from Kraichnan (1962); $\frac{\delta_m}{\delta_T}$ (laminar) from Bird et al. (1961)

$$\vec{q} = -k \frac{\partial T}{\partial y} = \frac{k(T_w - T_\infty)}{7y} \left(\frac{y}{\delta}\right)^{1/7} \quad (103)$$

$$\vec{q}_w = -k \left.\frac{\partial T}{\partial y}\right|_{y=0} = \frac{k(T_w - T_\infty)}{r} Nu \quad (104)$$

and finally

$$Nu = 0.13\ Ra^{1/3} \quad (105)$$

Discussion

Several significant conclusions come from an analysis of the computational results tabulated in Table 16. Firstly, Ra numbers seem to exceed the critical value of about 10^{10} (above which there is turbulence) in spite of the rather small flow volumes. Even reducing $(T_\infty - T_w)$ by a factor of 10 (e.g., $T_\infty - T_w = 20°C$) will not alter the conclusion that magmas rising through the mantle should be fairly well mixed. This is especially true when they ascend through relatively cool volumes of mantle. In the case of turbulent mixing, energy losses may be large enough to crystallize significant portions of the diapir thereby reducing buoyancy forces and effectively ending ascent. From a heat transfer point of view it is interesting to note that for constant Ra the convective heat losses sustained by a rising diapir are 3 to 5 times greater for turbulent flow than for laminar. The assumption of adiabatic rise is often made in petrologic arguments. As can be seen however, this assumption can be in error even for the rapidly ascending bodies calculated in Table 16. The velocities calculated (for turbulence) are of the same order as the Stokes nodule settling rate and so the balance used earlier (equation 83) may not be totally appropriate for high Ra flow.

Mass Transfer Rates

We now turn to a calculation of the rate of mass transfer a rising diapir may be expected to experience in its ascent. In the source region, of course, the liquid is in chemical and thermal equilibrium with its surroundings. Once it separates from its residue however and begins to rise into a cooler environment chemical potential and thermal gradients will be established and hence the tendency for mass and energy exchange will exist. We have already calculated heat losses and have shown they can be important. Our aim now is to develop quantitative expressions for the rate of mass transfer for the various components. The authors recognize the fact that in general, multi-component diffusion can be a very complicated process with various species diffusing up their activity gradients; the only constraint on the system is that the total rate of entropy production be positive and a minimum if the classical linear phenomenological laws are being followed. In addition to these problems, the diffusion tensors for each component in silicate melts have not been determined consequently a rigorous treatment of multicomponent diffusion is beyond our means at the present time. As an alternative we treat the multicomponent silicate systems as pseudobinary systems to at least obtain an estimate of what mass fluxes may be important.

The equation of continuity for component i is given by (assuming constant ρ and D_i where D_i is the mass diffusivity of component i in the silicate melt and ignoring the non-steady term):

$$u \frac{\partial W_i}{\partial Z} = D_i \frac{\partial^2 W_i}{\partial y^2} \quad (106)$$

where W_i is the mass fraction of component i and u is the velocity in the boundary layer. Concentration boundary layers are much smaller than either δ_T or δ_M because typical D_i values are orders of magnitude smaller than either κ or ν. In fact it can be shown (Bird et al., 1960, p. 607) that

$$\delta_M = Sc^{1/3} \delta_c$$

where Sc, the Schmidt number, is defined as

$$Sc = \frac{\nu}{D} . \quad (107)$$

A typical value for Sc is

$$\sim 10^2/10^{-7} \simeq 10^9 .$$

Accordingly, we expect the diffusional front to lie entirely within the thermal and momentum boundary layers and therefore take (for laminar flow)

$$u = \frac{3u_{max}}{\delta} y \quad (108)$$

in equation (106) and

$$u = \frac{29u_{max}}{\delta} y \quad (109)$$

in equation (106) for turbulent flow. This is tantamount to assuming that velocities are linear functions of the y spatial coordinate within the thin chemical boundary layer. The boundary conditions for equation (106) are

B.C. 1 $\quad W = W_\infty$ at $y = \infty \quad (110)$

B.C. 2 $\quad W = W_w$ at $y = 0 \quad (111)$

B.C. 3 $\quad W = W_\infty$ at $Z = 0 \quad (112)$

The solution to equation (106) subject to the velocity distributions given by (108) and (109) and the boundary conditions (110 through (112) is given in the Appendix. The results for the mass flux at the wall are:

$$j_m^{\ell} = 1.12\ \rho_L D_i\ (W_w - W_\infty)\ \left(\frac{u_{max}}{3\delta r D_i}\right)^{1/3} \quad (113)$$

(laminar flow, ℓ)

$$j_m^{t} = 1.12\ \rho_L D_i\ (W_w - W_\infty)\ \left(\frac{29u_{max}}{9D_i \delta r}\right)^{1/3} \quad (114)$$

(turbulent flow, t)

These local rates may be used to calculate integral quantities (e.g., total mass gain or loss) in a

TABLE 17

Mass Transfer Rates

Component	$W_w - W_\infty$ (wt. fraction)	D_i ($cm^2 s^{-1}$)	j_m^l (gm $cm^{-2} s^{-1}$)	m_T^l (gm)	j_m^t (gm $cm^{-2} s^{-1}$)	m_T^t (gm)
Si	-.0142	8×10^{-7}	-5×10^{-8}	-7.1×10^{8}	-1.1×10^{-5}	-3×10^{9}
Ti	-.0187	7×10^{-7}	-6×10^{-8}	-8.5×10^{8}	-2.6×10^{-7}	-3.6×10^{9}
Al	-.120	5×10^{-7}	-3×10^{-7}	-4.2×10^{9}	-1.3×10^{-6}	-1.8×10^{10}
Fe	-.0163	9×10^{-7}	-6×10^{-8}	-8.5×10^{8}	-2.6×10^{-7}	-3.6×10^{9}
Mg	.288	4×10^{-7}	6×10^{-7}	8.5×10^{9}	2.6×10^{-6}	3.6×10^{10}
Ca	-.0588	5×10^{-7}	-2×10^{-7}	-2.8×10^{9}	-8.6×10^{-7}	-1.2×10^{10}
Na	-.0322	4×10^{-6}	-3.3×10^{-7}	-4.7×10^{9}	-1.4×10^{-6}	-2×10^{10}
K	-.0156	2×10^{-6}	-1×10^{-7}	-1.4×10^{9}	-4.3×10^{-6}	-6×10^{10}
H_2O	-.0100	1×10^{-7}	-8.7×10^{-9}	-1.2×10^{8}	-3.7×10^{-8}	-5×10^{8}
Ni	.002	9×10^{-7}	7.6×10^{-9}	1.1×10^{8}	3.2×10^{-8}	4.7×10^{8}
Sr	.002	9×10^{-5}	1.6×10^{-7}	2.3×10^{9}	6.9×10^{-7}	9.8×10^{9}
Cs	.002	2×10^{-6}	1.3×10^{-8}	1.8×10^{8}	5.6×10^{-8}	7.7×10^{8}

Estimates of convection diffusive mass fluxes and total mass exchange values for typical alkali basalt system are listed in the Table. The rate and integral quantities are calculated using equations (A17) and (A18) and estimates of the effective binary diffusivities from Winchell (1969), Shaw (1974), Medford (1973), Hoffman (1974), Varshneya and Cooper (1968, a and b), Cooper et al. (1967) and the present authors. $W_w - W_\infty$ is calculated by subtracting from the weight fractions of the various oxide components in pyrolite the corresponding quantity in CSQ-28. The diffusivities in column 3 are approximations to D at 1500°C for the various components in basic silicate melts. All values listed were calculated using u_{max} and δ values calculated by the hydrodynamic equations cited earlier and tabulated in Table 16. The parameters held constant are as follows:

$$Ra = 1.2 \times 10^{15}$$
$$Pr = 5 \times 10^{3}$$
$$\nu = 50\ cm^2 s^{-1}$$
$$V = 0.185\ Km^3$$
$$\rho_L = 2.75\ gm\ cm^{-3}$$
$$Z = 75\ Km$$
$$\omega = 10\ cm\ s^{-1}$$

Total magma mass = $\rho_L V = 2.5 \times 10^{14}$ gm

Negative fluxes and integral mass quantities refer to movement out of the magma into the surroundings. Columns 5 and 7 computed using equation 115 in the text.

fasion analogous to the temperature loss calculations previously performed. This procedure gives

$$m^t_{T,i} = \frac{SZ}{\omega} j^t_m \qquad (115)$$

$$m^\ell_{T,i} = \frac{SZ}{\omega} j^\ell_{m,i} \qquad (116)$$

where S is the total surface area (taken here as $4\pi r^2$) and Z and ω the ascent depth and rate respectively. Table 17 presents some quantitative estimates of the local rate and total mass flow for a number of silicate melt components. The diffusivity data has come from a number of sources, the reliability of which is difficult to estimate. Nevertheless we feel these data do give some idea of the approximate amount of mass transfer that might take place in the flow regimes discussed in this paper. The values for u_{max} and δ come from the equations given earlier in the heat transfer section and are the same values listed in Table 16. Several features may be noted by an examination of Table 17. Turbulent mass transfer rates tend to be higher by about a factor of 5 or so than the corresponding laminar values. There are three main reasons for this: (1) the maximum velocity in turbulent flow occurs closer to the boundary; (2) the turbulent boundary layer is thinner than the laminar one thereby reducing the effective distance a particle must travel to get into the well mixed zone and (3) turbulent velocities (at constant Ra, Pr and ν) are higher than laminar velocities. Integral values of mass exchange

$$(m^t_{T,i} \text{ or } m^\ell_{T,i})$$

are small in comparison to the total mass of the ascending diapir. For the case given in Table 17 for instance the total amount of magma is of order

3×10^{14} gms whereas the greatest integral value, the value of 4×10^{10} gms for MgO, represents a gain of only 0.15 wt. % MgO. It should be pointed out however, that these calculations depend inversely on the ascent velocity. If ω was 10 times smaller, for instance, mass transfer rates and integral quantities would be ten times higher. Note that for components in small amounts (such as certain radiogenic nuclides) advective diffusional mass transfer could play a significant role, especially if concentration differences were magnified for some reason. Although it appears that to first order the nodule bearing alkali basalts rise too quickly for any significant mass exchange these same equations and processes might find application to other magmatic systems. Marsh (1974) for example, calculated by energy balance methods similar to those used here, typical ascent times of 10^4 years for kilometer sized (radius) "andesitic" magma bodies rising from Benioff zones in island arc areas. A calculation of the u_{max} and δ from the dynamical equations and application of equations (A17) and (A18) shows that indeed there should be significant mass exchange; a little reflection makes the idea of relatively siliceous magmas ascending through something of the order of 100 km of peridotitic mantle with no compositional imprint seem a bit implausible.

In order to summarize the conclusions of the previous few sections, we attempt here to reconstruct the temperature-depth history of a specific sample -- CSQ-28. This sample has been chosen since the equilibration of CSQ-28 liquid and its megacryst assemblage has been calculated. There are three main contributions to the temperature loss of ascending alkalic basalt magma body sustains:

i) latent heat effects (equation 81 and Table 14)

ii) convective heat loss through boundary layer flow (equations 90-97 for laminar flow; equations 99-105 for turbulent flow, equation T16 and Table 16)

iii) heat effect associated with work done by expansion as the magma rises to lower pressure environment (i.e., the adiabatic work term).

For CSQ-28 we take as the starting point or point of beginning ascent, the previously calculated equilibration conditions with peridotite, namely

$$T_E = 1356°C$$

$$P_E = 24.1 \text{ Kbars } (Z_E = 77 \text{ Km})$$

The adiabatic temperature drop experienced by the magma body is given by

$$(\Delta T)^{\text{reversible}}_{\text{expansion}} = - T_E[1 - \text{EXP}(-\alpha g(Z-Z_E)/C_{P,L})] \simeq -47 \text{ K}$$

Assuming the volume of magma to be 0.03 km^3 and ω, the ascent rate to be on the average 10 cm s^{-1} we calculate from equation (68) an effective mantle viscosity of $\eta_m \sim 7.3 \times 10^9$ poise. Equations (73) and (74) then allow an estimate of (T-Ts) for periodotite of 277°C, the thickness of the partial melt zone being $\delta r \sim 12$ cm (equation 80). The temperature loss incurred by the magma (equation 81) is

$$(T_E - T)^{\text{latent}}_{\text{heat}} \simeq 54°C.$$

Application of the turbulent hydrodynamic equations enables us to estimate the convective heat loss for the system. We have, after application of equations (99), (100), (105) and (T16) (see legend Table 16)

$$(T_E - T)_{\text{convection}} \simeq 175°.$$

If these heat effects are distributed linearly over the ascent depth we estimate a total ΔT of -183°C over a length of 77 km for a linear temperature gradient of -2.4°C/km. We would predict a value of

$$T_E + (\Delta T)_{\text{heat loss}} = 1173°C$$

for the temperature at which the lava is erupted. At the depth of megacryst precipitation ($\sim$40 km) we would predict a temperature of 1267°C about 30°C higher than the calculated equilibration temperature. Considering the uncertainty in the thermodynamic and transport properties this discrepancy is not particularly unsettling.

Conclusions

We can think of no better statement to end this paper with than one written by H. R. Shaw in a paper published in 1965:

> In a sense, the preceding commentary may be construed as a catalogue of deficiencies in our knowledge of magmatic systems. These are perhaps about equally divided between insufficient quantitative data from the field and an inadequate foundation in theory and experiment for their interpretation. Many of the latter have been pointed out already, but it is the problem of quantitative measurements from the field that is perhaps the major obstacle in view of the difficulty and time required to carry out measurements in sufficient detail. The mechanistic approach to problems of magmatic evolution may seem to offer impossible goals, and consequently gathering data toward these ends seems fruitless. Consider, however, that it is precisely the elucidation of the mechanical process by which an igneous rock is produced that is one of the chief aims, usually only by implication, of petrogenetic studies. The work that is needed most is to extend observations of a kind already made as a routine part of petrologic studies, that is, formulate on a more quantitative basis the description of an igneous rock body with regard to all chemical, mineralogical, and textural variations within a quantitatively described geologic setting. These results can provide us with several guides to an interpretation of the mechanical history of the rock body.

To these comments we would only like to underscore the importance of viewing magmatic systems historically; that is as a succession of chemical and mechanical instabilities each operating with an appropriate time scale. The product of any given volcanic eruption is really the physical manifestation of the superposition of the various competing thermodynamic and thermomechanical processes operating in the Earth.

ACKNOWLEDGEMENTS

This research was supported by the National Science Foundation (GA-43771X), the United States Energy Research and Development Administration, the Committee on Research of the University of California, the Penrose Fund of the Geological Society of America and the National Research Council of Canada (A7372). We are particularly indebted to Dr. R. Hultgren for the use of his drop calorimeter and to Dr. C. Bacon for instruction in its use. Dr. H. R. Shaw provided guidance, criticism and continuous commentary.

APPENDIX

The equations we want to solve are

$$\frac{3u_m}{\delta} y \frac{\partial W_i}{\partial Z} = D_i \frac{\partial^2 W_i}{\partial y^2} \quad \text{(laminar flow)} \tag{A1}$$

$$\frac{29u_m}{\delta} y \frac{\partial W_i}{\partial Z} = D_i \frac{\partial^2 W_i}{\partial y^2} \quad \text{(turbulent flow)} \tag{A2}$$

subject to the boundary conditions

$$W = W_w \text{ at } y = 0$$

$$W = W_\infty \text{ at } y = \infty$$

Now, let

$$\beta_\ell = \frac{D\delta}{3u_{max}} \qquad \beta_t = \frac{D\delta}{29u_{max}} \tag{A3}$$

so that we have

$$y \frac{\partial W_i}{\partial Z} = \beta_\ell \frac{\partial^2 W_i}{\partial y^2} \tag{A4}$$

and an equation with β_t instead of β_ℓ for the turbulent case. In what follows we only deal with the laminar case; the turbulent results may be found by simply substituting β_t for β_ℓ.

We define the following reduced variables

$$C = \frac{W - W_\infty}{W_w - W_\infty} \quad \text{and} \quad \eta = y(9\beta z)^{-1/3}$$

and substituting these back into (A4) we have after some reduction

$$\frac{d^2C}{d\eta^2} + 3\eta^2 \frac{dC}{d\eta} = 0 \tag{A6}$$

$$\text{B.C.1.} \quad C = 0 \text{ as } \eta \to \infty$$

$$\text{B.C.2.} \quad C = 1 \text{ at } \eta = 0 \tag{A7}$$

Integrating [A6) once gives

$$\frac{dC}{d\eta} = B_1 e^{-\eta^3} \tag{A8}$$

which may be integrated again to give

$$C = B_1 \int_0^\eta e^{-\eta^3} d\eta + B_2 \tag{A9}$$

Applying the boundary conditions to (A9) we solve for the constants B_1 and B_2. This gives

$$B_1 = 1 \tag{A10}$$

$$B_1 = -\left[\int_0^\infty e^{-\eta^3} d\eta\right]^{-1} \tag{A11}$$

The definite integral is well known, being the value of the Gamma function

$$\Gamma(4/3) = 1/3\ \Gamma(1/3) = 0.893 \tag{A12}$$

The final result for the mass distribution becomes

$$C = \frac{\int_0^\infty e^{-\eta^3} d\eta}{\int_0^\infty e^{-\eta^3} d\eta} + 1 = 1 - 1.12 \int_0^\eta e^{-\eta^3} d\eta \tag{A13}$$

The rate of mass flux at the wall entering the magma body is obtained as follows

$$j_{m,i} = -\rho_L D_i \frac{dW}{dy} = -\rho D_i \frac{\partial W}{\partial c} \frac{\partial c}{\partial \eta} \frac{\partial \eta}{\partial y} \tag{A14}$$

$$= -\rho_L D_i (W_w - W_\infty) \frac{\eta}{y} \frac{dc}{d\eta} \tag{A15}$$

$$j_{m,i} = \frac{+\rho_L D_i (W_w - W_\infty)}{\Gamma(4/3)} \left(\frac{u_{max}}{3D_i \delta Z}\right)^{1/3} \exp\left[\frac{-u_{max}\, y^3}{3\delta\, D_i Z}\right] \tag{A16}$$

At the wall, y = 0 (recall that y is positive into the magma) and letting r be the reference length scale we have

$$j^\ell_{m,i} = 1.12\ \rho_L D_i (W_w - W_\infty) \left(\frac{u_{max}}{3D_i \delta r}\right)^{1/3} \tag{A17}$$

(laminar flow)

and

$$j^t_{m,i} = 1.12\ \rho_L D_i (W_w - W_\infty) \left(\frac{29\ u_{max}}{9D_i \delta r}\right)^{1/3} \tag{A18}$$

(turbulent flow)

j_m is measured in gms $cm^{-2}s^{-1}$.

REFERENCES

Aoki, K. and Shiba, I., 1943, Pyroxenes from lherzolite inclusions of Itinomegata, Japan. Lithos 6, 41-52.

Arculus, R. J., 1975, Melting behavior of two basanites in the range 10-35 kbar and the effect of TiO_2 on the olivine-diopside reactions at high pressures. Carnegie Inst. Wash. Yb. 74, 512-515.

Arculus, R. J., and Shimizu, N., 1947, Rare earth elements in a suite of basanitoids and alkali olivine basalts from Grenada, Lesser Antilles. Carnegie Inst. Wash. Yb, 73, 553-560.

Arndt, J. and Häberle, F., 1973, Thermal expansion and glass transition temperatures of synthetic glasses of plagioclase-like compositions. Contr. Mineral. Petrol. 39, 175-183.

Bacon, C. R., 1976, High temperature heat content and heat capacity of silicate glasses: experimental determination and a model for calculation. Amer. Jour. Sci. in press.

Bacon, C. R. and Carmichael, I. S. E., 1973, Stages in the P-T path of ascending basalt magma: An example from San Quintin, Baja California. Contr. Mineral. Petrol. 41, 1-22.

Batchelor, G. K., 1967, An introduction to fluid dynamics. Cambridge: Cambridge University Press. 615 pp.

Bennett, F. D., 1971, Vaporization waves in explosive volcanism, Nature 234, 538-539.

Binns, R. A., Duggan, M. B., and Wilkinson, J. F. G., 1970, High-pressure magacrysts in alkaline lavas from northeastern New South Wales. Amer. Jour. Sci. 269, 132-168.

Birch, F., 1966, Compressibility; elastic constants. In Handbook of Physical Constants, S. P. Clark, Jr., ed. Geol. Soc. Am. Mem. 97-173.

Bird, R. B., Stewart, W. E. and Lightfoot, E. N., 1960, Transport Phenomena. New York: John Wiley and Sons, 780 pp.

Bottinga, Y. A., and Weill, D. F., 1970, Densities of liquid silicate systems calculated from partial molar volumes of oxide components. Amer. Jour. Sci. 269, 169-182.

Boyd, F. R., 1969, Electron microprobe study of diopside inclusions from kimberlite. Amer. Jour. Sci. 267A, 50-69.

Boyd, F. R., 1973, A pyroxene geotherm. Geochim. et Cosmochim. Acta 37, 2533-2546.

Boyd, F. R. and England, J. L., 1963, Effect of pressure on the melting of diopside, $CaMgSi_2O_6$, and albite, $NaAlSi_3O_8$, in the range up to 50 kilobars. Jour. Geophys. Res. 68, 311-323.

Brown, F. H., 1971, Volcanic petrology of the Toro-Ankole region, Western Uganda. Ph.D. thesis, University of California, Berkeley, 152 pp.

Brown, F. H. and Carmichael, I. S. E., 1971, Quaternary volcanoes of the Lake Rudolf region: II The lavas of North Island, South Island, and the Barrier. Lithos 4, 305-323.

Buddington, A. F. and Lindsley, D. H., 1964, Iron-titanium oxide minerals and synthetic equivalents. Jour. Petrol. 5, 310-357.

Bultitude, R. J. and Green, D. H., 1971, Experimental study of crystal-liquid relationships at high pressures in olivine nephelinite and basanite compositions. Jour. Petrol. 12, 121-147.

Burnham, C. W., 1975, Water and magmas; a mixing model. Geochim. et Cosmochim. Acta 39, 1077-1084.

Burnham, C. W. and Davis H. F., 1971, The role of H_2O in silicate melts I. P-V-T relations in the system $NaAlSi_3O_8$ - H_2O to 10 kilobars and 1000°C. Amer. Jour. Sci. 270, 54-79.

Burnham, C. W. and Davis, H. F., 1974, The role of H_2O in silicate melts: II. Thermodynamic and phase relations in the system $NaAlSi_3O_8$ - H_2O to 10 kilobars, 700° to 1100°C. Amer. Jour. Sci. 274, 902-940.

Carmichael, I. S. E., 1967a The mineralogy and petrology of the volcanic rocks from the Leucite Hills, Wyoming. Contr. Mineral. Petrol. 15, 24-66.

Carmichael, I. S. E., 1967b, The mineralogy of Thingmuli, a Tertiary volcano in Eastern Iceland. Amer. Mineral. 52, 1815-1841.

Carmichael, I. S. E., Turner, F. J., and Verhoogen, J., 1974, Igneous Petrology. New York: McGraw Hill, 739 pp.

Carslaw, H. S., and Jaeger, J. C., 1959, Conduction of Heat in Solids, 2nd ed., Oxford Univ. Press, London.

Charlu, T. V., Newton, R. C., and Kleppa, O. J., 1975, Enthalpies of formation at 970 K of compounds in the system MgO-Al_2O_3-SiO_2 from high temperature solution calorimetry. Geochim. et Cosmochim.Acta 39, 1487-1497.

Chandrasekkar, S., 1961, Hydrodynamics and Hydromagnetic Stability. New York: Oxford University Press.

Cooper, A. R. and Varshenya, A. K., 1968, Diffusion in the system K_2O-SrO-SiO_2: I. Effective binary diffusion coefficients. Jour. Amer. Ceram. Soc. 51, 103-106.

Dawson, J. B., Powell, D. G. and Reid, A. M., 1970, Ultrabasic xenoliths and lava from the Lashaine Volcano, Northern Tanzania. Jour. Petrol. 11, 519-548.

Eckert, E. G. and Jackson, T. W., 1950, Nat. Advisory Comm. Aeronaut. Tech. Note 2207.

Eggler, D. H., 1972, Water saturated and unsaturated melting relations in a Paricutin Andesite and an estimate of water content in the natural magma. Contr. Mineral. Petro. 34, 261-271.

Eggler, D.H., 1975, Peridotite-carbonate relations in the system CaO-MgO-SiO_2-CO_2. Carnegie Inst. Wash. Yb. 74, 468-474

Fairzullaev, D., 1969, Laminar motion of multiphase media in conduits. New York: Consultants Bureau, 144 pp.

Ferrier, A., 1970, Kristallisationswärme von diopsid. Ber. Dt. Keram. Ges. 47, 64-67.

Flood, H., and Knapp, W. J., 1968, Structural characteristics of liquid mixtures of feldspars and silica. Jour. Amer. Ceram. Soc. 51, 259-263.

Flower, M. F. J., 1971, Evidence for the role of phlogopite in the genesis of alkali basalts. Contr. Mineral. Petrol. 32, 126-137.

Ganguly, J., 1973, Activity-composition relations of jadeite in omphacite pyroxene: theoretical deductions. Earth and Planet. Sci. Lett. 19, 145-153.

Gast, P. W., 1968, Trace element fractionation and the origin of tholeiitic and alkaline magma types. Geochim. et Cosmochim. Acta 32, 1057-1086.

Goldstein, S., 1938, Modern Developments in Fluid Mechanics, 2. Oxford: Clarendon Press.

Greene, D. H., 1970, The origin of basaltic and nephelinitic magmas. Trans. Leicester Lit. Phil. Soc. 64, 26-54.

Green, D. H., 1973a, Conditions of melting of basanite magma from garnet peridotite. Earth Planet. Sci. Lett. 17, 456-465.

Green, D. H., 1973b, Experimental melting studies on a model upper mantle composition at high pressure under water-saturated and water-undersaturated conditions. Earth Planet. Sci. Lett. 19, 37-53.

Green, D. H. and Hibberson, W. O., 1970, Experimental duplication of conditions of precipitation of high pressure phenocrysts in a basaltic magma. Phys. Earth and Planet. Int. 3, 247-254.

Green, D. H., and Ringwood, A. E., 1967, The genesis of basaltic magmas. Contr. Mineral. Petrol. 15, 103-190.

Gruntfest, I. J., 1963, Thermal feedback in liquid flow; plane shear at constant stress. Trans. Soc. Rheol. 7, 195-207.

Hallman, T. M., 1956, Combined forced and free-laminar transfer in vertical tubes with uniform internal heat generation. Trans. ASME 78, 1831-1840.

Hamilton, D. L., Burnham, C. W., and Osborn, E. F., 1964, The solubility of water and effects of oxygen fugacity and water content on crystallization in mafic magmas. Jour. Petrol. 5, 21-39.

Heming, R. F., and Carmichael, I. S. E., 1973, High-temperature pumice flows from the Rabaul Caldera, Papua New Guinea. Contr. Mineral. Petrol. 38, 1-20.

Hensen, B. J., Schmid, R., and Wood, B. J., 1975, Activity-composition relationships for pyrope-grossular garnet. Contr. Mineral. Petrol. 51, 161-166.

Hoffman, A., 1974, Dept. Terrestrial Magnetism, Carnegie Inst. Wash. Yb. 74, p. 183.

Holloway, J. R., 1973, The system pargasite - H_2O-CO_2: a model for melting of a hydrous mineral with a mixed volatile fluid - I. Experimental results to 8 kbar. Geochim. et Cosmochim. Acta 37, 651-66.

Irving, A. J., 1974, Megacrysts from the newer basalts and other basaltic rocks of south-eastern Australia. Geol. Soc. Amer. Bull. 85, 1503-1514.

JANAF, 1971, JANAF Thermochemical Tables 2nd ed. Nat. Stand. Ref. Data Ser., Nat. Bur. Stand.(US) 37. 1141 pp.

JANAF, 1974, JANAF Thermochemical Tables, 1974, Supplement. Jour. Phys. Chem. Ref. Data 3, 311-480.

JANAF, 1975 JANAF Thermochemical Tables, 1975, Supplement. Jour. Phys. Chem. Ref. Data 4, 1-175.

Janz, G. J., 1967, Molten salts handbook. Academic Press, Inc., New York.

Jessup, R. S., 1955, A new bunsen-type calorimeter. Jour. Res. Nat. Bur. Stds. 55, 317-322.

Kay, J. M., 1968, An Introduction to Fluid Mechanics and Heat Transfer 2nd ed. Cambridge: Cambridge University Press, 327 pp.

Kay, R. W. and Gast, P. W., 1973, The rare earth content and origin of alkali-rich basalts. Jour. Geol. 18, 653-682.

Kelley, K. K., 1960, Contributions to the data on theoretical metallurgy: Pt. 13, high temperature heat content, heat capacity and entropy data for the elements and inorganic compounds. U. S. Bur. Mines Bull. 584, 232 pp.

Kerrick, D. M., and Darken, L. S., 1975, Statistical thermodynamic models for ideal oxide and silicate solid solutions with applications to plagioclase. Geochim. et Cosmochim. Acta 39, 1431-1442.

King, E. G., Orr, R. L., and Bonnickson, K. R., 1954, Low temperature heat capacity, entropy at 298.16°K., and high temperature heat content of sphene ($CaTiSiO_5$). Jour. Am. Chem. Soc. 76, 4320-4321.

Kirshenbaum, A. D. and Cahill, J. A., 1960, The density of liquid aluminum oxide. Jour. Inorg. Nucl. Chem. 14, 283-287.

Klein, L. and Uhlman, D. R., 1974, Crystallization behavior of anorthite. Jour. Geophys. Res. 79, 4869-4874.

Klotz, I. R., 1964, Chemical Thermodynamics, New York: W. A. Benjamin Inc., 468 pp.

Kraichnan, R. H., 1962, Turbulent thermal convection at arbitrary Prandtl number. Phys. Fluids 5, 1374-1389.

Kudo, A. M., and Weill, D. F., 1970, An igneous plagioclase thermometer. Contr. Mineral. Petrol. 25, 52-65.

Kushiro, I., Shimizu, N., Nakamura, Y., and Akimoto, S., 1972, Compositions of coexisting liquid and solid phases formed upon melting of natural garnet and spinel lherzolites at high pressures: A preliminary report. Earth Planet. Sci. Lett. 14, 19-25.

Lacy, E. D., 1955, Atomic packing in silicate glasses, in The Vitreous State; Glass Delegacy, University of Sheffield, England, 23-46.

Lamb, H., 1945, Hydrodynamics, 6th Ed., Dover Publications, New York.

Leu, A., Ma, S., and Eyring, H., 1975, Properties of molten magnesium oxide. Proc. Nat. Acad. Sci. U.S.A. 72, 1026-1030.

Lighthill, M. J., 1953, Theoretical considerations on free convection in tubes. Quat. Jour. Mech. Appl. Math. 6, 398-439.

Lindsley, D. H., 1966, Melting relations of $KAlSi_3O_8$: effect of pressures up to 40 kilobars. Amer. Mineral. 51, 1793-1799.

Lindsley, D. H., 1967, Pressure-temperature relations in the system $FeO-SiO_2$. Carnegie Inst. Wash. Yb.65, 226-230.

Lumsden, J., 1961, The thermodynamics of liquid iron silicates, in Physical Chemistry of Process Metallurgy. Metal. Soc. Conf. 7, New York: Interscience, Inc.

MacDonald, G. A., 1949, Petrography of the island of Hawaii., U.S.G.S. Prof. Paper 214-D, 51-96.

MacGregor, I. D., 1969, The system $MgO-SiO_2-TiO_2$ and its bearing on the distribution of TiO_2 in basalts. Amer. Jour. Sci. 267-A, 342-363.

MacGregor, I. D., and Basu, A. R., 1974, Thermal structure of the lithosphere: a petrologic model. Science 185, 1007-1011.

Mah, A. D., 1960, Thermodynamic properties of manganese and its compounds. U. S. Bureau of Mines Report of Investigations 5600, 34 pp.

Marsh, B. D., 1974, Aleutian Island arc magmatism. Ph.D. thesis, University of California, Berkeley.

McNown, J. S. and Malaika, J., 1950, Effects of particle shape on settling velocity at low Reynolds numbers. Amer. Geophys. Union Trans. 31, 74-82.

Medford, G. A., 1973, Calcium diffusion in a mugearite melt. Can. Jour. Earth Sci. 10, 394-402.

Mercier, J. C., and Carter, N. L., 1975, Pyroxene geotherms. Jour. Geophys. Res. 80, 3349-3362.

Meyer, H. O. A. and Boyd, F. R., 1972, Composition and origin of crystalline inclusions in natural diamonds. Geochim. et Cosmochim. Acta 36, 1255-1273.

Meyers, G. E., 1971, Analytical Methods in Conduction Heat Transfer. New York: McGraw-Hill.

Millhollen, G. L., Irving, A. J., and Wyllie, P. J., 1974, Melting interval of peridotite with 5.7 percent water to 30 kilobars. Jour. Geol. 82, 575-587.

Moore, J. G., 1970, Water content of basalt erupted on the ocean floor. Contr. Mineral. Petrol. 28, 272-279.

Morton, B. R., 1960, Laminar convection in uniformly heated vertical pipes. Jour. Fluid Mech. 8, 227-240.

Mysen, B. and Boettcher, A. L., 1975, Melting of a hydrous mantle II. Geochemistry of crystals and liquids formed by anatexis of mantle peridotite at high pressures and temperatures as a function of controlled activities of water, hydrogen, and carbon dioxide. Jour. Petrol. 16, 549-593.

Nafziger, R. H., 1973, High-temperature activity composition relations of equilibrium spinels, olivines and pyroxenes in the system $MgO-Fe-SiO_2$. Amer. Mineral. 58, 457-465.

Navrotsky, A., 1971, The intracrystalline cation distribution and the thermodynamics of solid solution formation in the system $FeSiO_3-MgSiO_3$, Amer. Mineral. 56, 201-211.

Naylor, B. F., 1945, High temperature heat contents of sodium metasilicate and sodium disilicate. Jour. Amer. Ceram. Soc. 41, 461-463.

Nehru, C. G., and Wyllie, P. J., 1974, Electron microprobe measurement of pyroxenes coexisting with H_2O-saturated liquid in the join $CaMgSi_2O_6-Mg_2Si_2O_6$ at 30 kilobars with application to geothermometry. Contr. Mineral. Petrol. 48, 221-228.

Nicholls, I. A. and Ringwood, A. E., 1973, Effect of water on olivine stability in thoeiites and the production of silica-saturated magmas in the island arc environment. Jour. Geol. 81, 285-300.

Nicholls, J., and Carmichael, I. S. E., 1972, The equilibration temperature and pressure of various lava types with spinel and garnet peridotite. Amer. Mineral. 57, 941-959.

Nicholls, J., Carmichael, I. S. E., and Stormer, J., 1971, Silica activity and P_{total} in igneous rocks. Contr. Mineral Petrol. 33, 1-20.

Nicolis, G., Prigogine, I. and Glansdorff, p. 175 On the mechanism of instabilities in nonlinear systems. Advances in Chemical Physics 32, 1-11.

O'Hara, M. J., Richardson, S. W. and Wilson, G., 1971, Garnet-peridotite stability and occurrence in crust and mantle. Contr. Mineral. Petrol. 32, 48-68.

Onions, R. K. and Grönwold,K., 1973, Petrogenetic relationship of acid and basic rocks in Iceland: Sr isotopes and rare-earth elements in late and postglacial volcanics. Earth Planet. Sci. Lett. 19, 397-409.

Orr, R. L., 1953, High-temperature heat contents of magnesium orthosilicate and ferrous orthosilicate. Jour. Amer. Chem. Soc. 75, 528-529.

Ostrach, S. and Thornton, P. R., 1958. On the stagnation of natural-convection flows in closed-end tubes. Trans. ASME 80, 363-366.

Pankratz, L., 1968, High temperature heat contents and entropies of dehydrated analcite, kaliophilite and leucite. U. S. Bur. Mines Dept. Invest. 7201.

Prigogine, I. and Defay, R., 1954, Chemical Thermodynamics, D. H. Everett, trans. Longmans, Green and Co., Ltd., London.

Prigogine, I. and Lefever, R., 1975, Stability and self-organization in open systems. Advances in Chemical Physics 24, 1-28.

Ramberg, H., 1968, Mantle diapirism and its tectonic and magmagenetic consequences. Phys. Earth Planet. Interior 5, 45-60.

Reece, A.W., 1961, Explanation of the geology of sheet 76 (Buhwezu). Geol. Surv. Uganda Rep. 4, 76pp.

Robie, R.A., Bethke, P.M. and Beardsley, K.M.,1967, Selected X-ray crystallographic data, molar volumes, and densities of minerals and related substances. U.S.G.S. Bull. No. 1248, 87 pp.

Robie, R. A. and Waldbaum, D. R., 1968, Thermodynamic properties of minerals and related substances at 298.15°K (25.0°C) and one atmosphere (1.013 bars) pressure and at higher temperatures. U.S.G.S. Bull. No. 1259, 256 pp.

Rosenhauer, M. and Eggler, D. H., 1975, Solution of H_2O and CO_2 in diopside melt. Carnegie Inst. Wash. Yb. 74, 474-479.

Rohsenow, W.M. and Choi, H. Y., 1962, Heat, Mass and Momentum Transfer. New Jersey: Prentice-Hall, 537 pp.

Rowlinson, J. S., 1969, Liquids and Liquid Mixtures, 2nd ed. Butterworth and Co., Ltd., London. 371 pp.

Scarfe, C. M., 1973, Water solubility in basic and ultrabasic magmas. Nature Phys. Sci. 246, 9-11.

Scheele, G. F. and Hanratty, T. J., 1962, Effect of natural convection on stability of flow in a vertical pipe. Jour. Fluid Mech. 14, 244-256.

Scherer, G., Hopper, R. W. and Uhlman, D. R., 1972, Crystallization behavior and glass formation of selected lunar compositions. Proceedings of the Third Lunar Science Conference, Geochim. et Cosmochim. Acta Suppl. 3, 2627-2637.

Schweite, H. E. and Ziegler, G., 1955, Beitrag zur specifichen wärme der gläser. Glastech. Ber. 28, 137-146.

Shaw, H. R., 1965, Comments on viscosity, crystal settling, and convection in granitic systems. Amer. Jour. Sci. 263, 120-152.

Shaw, H. R., 1969, Rheology of basalt in the melting range. Jour. Petrol. 10, 510-535.

Shaw, H. R., 1972, Viscosities of magmatic silicate liquids: an empirical method of prediction. Amer. Jour. Sci. 272, 870-893.

Shaw, H. R., 1973, Mantle convection and volcanic periodicity in the Pacific; evidence from Hawaii. Geol. Soc. Amer. Bull. 84, 1505-1527.

Shaw, H. R., 1974, Diffusion of H_2O in granitic liquids. Part I, Experimental data; Part II, Mass transfer in magma chambers, in A. W. Hoffman, B. J. Gilletti, H. S. Yoder and R. A. Gund eds. Geochemical Transport and Kinetics. Proceedings of a Conference held at Airlie Warrenton, Virginia, June 1973. Carnegie Inst. Wash., 139-170.

Shpil'rain, E.E. Kagan, D.N. and Barkhatov, L.S., 1972, Thermodynamic properties of the condensed phase of alumina near the melting point. High Temperatures-High Pressures 4, 605-609

Skinner, B. J., 1966, Thermal Expansion, in Handbook of Physical Constants. S. P. Clark, Jr., ed. Geol. Soc. Am. Mem. 97, 75-96.

Slagle, O. D., and Nelson, R. P., 1970, Adiabatic compressibility of molten alumina. Jour. Amer. Ceram. Soc. 53, 637-638.

Sleep, N. H., 1974, Segregation of magma from a mostly crystalline mush. Geol. Soc. Amer. Bull. 85, 1225-1232.

Smith, A. L. and Carmichael, I. S. E., 1968, Quaternary lavas from the southern Cascades, Western U.S.A. Contr. Mineral. Petrol. 19, 212-238.

Smith, A. L. and Carmichael, I. S. E., 1969, Quaternary trachybasalts from Southeastern California. Amer. Mineral. 54, 909-923.

Smith, D., 1970, Stability of iron-rich orthopyroxene. Carnegie Inst. Wash. Yb. 68, 229-231.

Sommerville, I.D., Ivanchev, I. and Bell, H.B.,1973 quoted from: Richardson, F.D. 1974, Physical Chemistry of Melts in Metallurgy vol. 1, Academic Press, London, 289 pp.

Spera, F. J., 1974, A thermodynamic basis for predicting water solubilities in silicate melts and implications for the low velocity zone. Contr. Mineral. Petrol. 45, 175-186.

Spera, F. J. and Hildreth, W., 1974, Activity of H_2O in undersaturated silicate liquids: petrogenetic implications. (Abs) Geol. Soc. Amer. Abst. with Prog. 6, 964.

Spil'rain, E. E., Kagan, D. N., and Barkhatov, L. S., 1972, Thermodynamic properties of the condensed phase of alumina near the melting point. High Temperatures-High Pressures 4, 605-609.

Stuckless, J.S. and Erickson, R.L., 1976, Strontium isotopic geochemistry of the volcanic rocks and associated megacrysts and inclusions from Ross Island and vicinity, Antarctica. Contr. Mineral. Petrol. (in press).

Stuckless, J. S. and Irving, A. J., 1976, Strontium isotope geochemistry of magacrysts and host basalts from Southeastern Australia. Geochim. et Cosmochim. Acta 40, 209-213.

Stormer, J. C., Jr., 1973, Calcium zoning in olivine and its relationship to silica activity and pressure. Geochim. et Cosmochim. Acta 37, 1815-1821.

Stueber, A. M., and Ikramuddin, M., 1974, Rubidium, strontium and the isotopic composition of strontium in ultramafic nodule minerals and host basalts. Geochim. et Cosmochim. Acta 38, 207-216.

Sutterby, J. L., 1973, Falling sphere viscometry. I. Wall and inertial corrections to Stokes' Law in long tubes. Trans. Soc. Rheology 17, 559-573.

Varshenya, A. K. and Cooper, A. R., 1972a, Diffusion in the system K_2O-SrO-SiO_2: II. Cation self-diffusion coefficients. Jour. Amer. Ceram. Soc. 55, 220-223.

Varshenya, A.K. and Cooper, A. R., 1972b, Diffusion in the system K_2O-SrO-SiO_2: III. Interdiffusion coefficients. Jour. Amer. Ceram. Soc. 55, 312-317.

Verhoogen, J., 1962, Oxidation of iron-titanium oxides in igneous rocks. Jour. Geol. 70, 168-181.

Weertman, J., 1971, Theory of water-filled crevices in glaciers applied to vertical magma transport beneath oceanic ridges. Jour. Geophys. Res. 76, 1171-1183.

Weill, D. F. and Drake, M. J., 1973, Europium anomaly in plagioclase feldspar: Experimental results and semi-quantitative model. Science 180, 1059-1060.

Whitehead, J. A. and Luther, D. S., 1975, Dynamics of laboratory diapirs and plume models. Jour. Geophys. Res. 80, 705-717.

Williams, R. J., 1971, Reaction constants in the system Fe-MgO-SiO_2-O_2 at 1 atm. between 900°C and 1300°C: Experimental results. Amer. Jour. Sci. 270, 334-360.

Williams, R. J., 1972, Activity-composition relations in the fayalite-forsterite solid solution between 900°C and 1300°C at low pressure. Earth and Planet. Sci. Lett. 15, 296-300.

Wilshire, H. G. and Jackson, E. D., 1975, Problems in determining mantle geotherms from pyroxene compositions of ultramafic rocks. Jour. Geol. 83, 313-329.

Winchell, P., 1969, The compensation law for diffusion in silicates. High Temp. Sci. 1, 200-215.

Wones, D. R., and Gilbert, M. E., 1969, The fayalite-magnetite-quartz assemblage between 600°C and 800°C. Amer. Jour. Sci. 267-A, 480-488.

Wood, B. J., and Strens, R. G. J., 1971, The orthopyroxene geobarometer. Earth and Planet. Sci. Lett. 11, 1-6.

Wrasidlo, W., 1974, Thermal analysis of polymers. Advances in Polymer Science 13. Berlin: Springer-Verlag, 99 pp.

Wright, T. L. and Weiblen, P. W., 1967, Mineral composition and paragenesis in tholeiitic basalt from Makaopuhi lava lake, Hawaii (abs.) An. Mtg. Geol. Soc. Amer. 1967, Program, New Orleans, 242 pp.

TECHNICAL INFORMATION DIVISION
LAWRENCE BERKELEY LABORATORY
UNIVERSITY OF CALIFORNIA
BERKELEY, CALIFORNIA 94720